Differential Scanning Calorimetry Techniques: Applications in Biology and Nanoscience

Pooria Gill,[1] Tahereh Tohidi Moghadam,[1] and Bijan Ranjbar[1,2,]*

Departments of [1]Nanobiotechnology and [2]Biophysics, Faculty of Biological Sciences, Tarbiat Modares University, Tehran, Iran

This paper reviews the best-known differential scanning calorimetries (DSCs), such as conventional DSC, microelectromechanical systems-DSC, infrared-heated DSC, modulated-temperature DSC, gas flow-modulated DSC, parallel-nano DSC, pressure perturbation calorimetry, self-reference DSC, and high-performance DSC. Also, we describe here the most extensive applications of DSC in biology and nanoscience.

KEY WORDS: DSC, MEMS-DSC, IR-heated DSC, MTDSC, GFMDSC, PNDSC, PPC, SRDSC, HPer DSC, structural transition, biothermodynamics

INTRODUCTION

Calorimetry is a primary technique for measuring the thermal properties of materials to establish a connection between temperature and specific physical properties of substances and is the only method for direct determination of the enthalpy associated with the process of interest.[1,2] Calorimeters are used frequently in chemistry,[3] biochemistry,[4,5] cell biology,[6] biotechnology,[7] pharmacology,[8] and recently, in nanoscience[9] to measure thermodynamic properties of the biomolecules and nano-sized materials. Amongst various types of calorimeters, differential scanning calorimeter (DSC) is a popular one. DSC is a thermal analysis apparatus measuring how physical properties of a sample change, along with temperature against time.[10] In other words, the device is a thermal analysis instrument that determines the temperature and heat flow associated with material transitions as a function of time and temperature.[11] During a change in temperature, DSC measures a heat quantity, which is radiated or absorbed excessively by the sample on the basis of a temperature difference between the sample and the reference material.[10,11]

Based on the mechanism of operation, DSCs can be classified into two types: heat-flux DSCs and power-compensated DSCs.[11] In a heat flux DSC, the sample material, enclosed in a pan, and an empty reference pan are placed on a thermoelectric disk surrounded by a furnace.[11,12] The furnace is heated at a linear heating rate, and the heat is transferred to the sample and reference pan through the thermoelectric disk.[11,12] However, owing to the heat capacity (C_p) of the sample, there would be a temperature difference between the sample and reference pans, which is measured by area thermocouples, and the consequent heat flow is determined by the thermal equivalent of Ohm's law:

$$q = \Delta T/\mathrm{R},$$

where q is "sample heat flow", ΔT is "temperature difference between sample and reference", and R is "resistance of thermoelectric disk".[12]

In a power-compensated DSC, the sample and reference pans are placed in separate furnaces heated by separate heaters.[11,13] The sample and reference are maintained at the same temperature, and the difference in thermal power required to maintain them at the same temperature is measured and plotted as a function of temperature or time.[11]

In the last decades, various DSC-based techniques have been developed to improve the molecular measurements of biomolecules. The best known of them are conventional/basic DSC,[14] microelectromechanical systems (MEMS)-DSC,[15] infrared (IR)-heated DSC,[16] modulated-temperature DSC (MTDSC),[17] gas flow-modulated DSC (GFMDSC),[18] parallel-nano DSC (PNDSC),[19] pressure perturbation calorimetry (PPC),[20] self-reference DSC (SRDSC),[21] and high-performance (HPer) DSC.[22] There are several reports of DSC applications in the literature for determining structural-phase transition,[23] melting point,[24] heat of fusion,[25] percent of crystallinity,[26] crystallization kinetics and phase transitions,[27] oxidative stability,[28] thermodynamical analysis of biomolecules,[29–31] and curing kinetics of nonbiological materials.[32] In this review, we describe various kinds of

*ADDRESS CORRESPONDENCE TO: Dr. Bijan Ranjbar, Departments of Nanobiotechnology and Biophysics, Faculty of Biological Sciences, Tarbiat Modares University, P.O. Box 14115-175, Tehran, Iran (Phone: +982182882005; Fax: +982188007598; E-mail: ranjbarb@modares.ac.ir)

DSC techniques and their applications in biology and nanoscience.

DSC

Definition

DSC is a thermodynamical tool for direct assessment of the heat energy uptake, which occurs in a sample within a regulated increase or decrease in temperature. The calorimetry is particularly applied to monitor the changes of phase transitions.[33,34]

DSC is commonly used for the study of biochemical reactions, which is named as a single molecular transition of a molecule from one conformation to another.[33] Thermal transition temperatures (T_t; melting points) of the samples are also determined in solution, solid, or mixed phases such as suspensions.[34]

In a basic DSC experiment, energy is introduced simultaneously into a sample cell (which contains a solution with the molecule of interest) and a reference cell (containing only the solvent). Temperatures of both cells are raised identically over time. The difference in the input energy required to match the temperature of the sample to that of the reference would be the amount of excess heat absorbed or released by the molecule in the sample (during an endothermic or exothermic process, respectively).[35–38] As a result of the presence of the molecule of interest, more energy is required to bring the sample to the same temperature as the reference; hence, the concept of heat excess comes into the picture (Fig. 1).

As a powerful analytical tool, DSC is capable of elucidating the factors that contribute to the folding and stability of biomolecules.[33] Changes in the C_p are believed to originate from the disruption of the forces stabilizing native protein structure. For example, this includes van der Waals, hydrophobic, and electrostatic interactions, hydrogen bonds, hydration of the exposed residues, conformational entropy, and the physical environment (such as pH, buffer, ionic strength, excipients).[38] Therefore, thermodynamic parameters obtained from DSC experiments are quite sensitive to the structural state of the biomolecule. Any change in the conformation would affect the position, sharpness, and shape of transition(s) in DSC scans.

Thermodynamic Terms

In a DSC experiment, thermodynamic parameters are associated with heat-induced macromolecular transitions. For a typical macromolecule, the molar C_p is measured as a function of temperature, subsequently, yielding the following thermodynamic parameters:

The partial C_p of a molecule

DSC measures the partial C_p of a sample. The C_p of the solution containing a macromolecule is measured with respect to the C_p of buffer in the absence of macromolecules. Hence, the instrument measures only part of what could be actually measured, which is the difference between sample and reference cells. The sample could be a protein, tRNA, a protein-DNA complex, a protein-lipid complex, or something else.[10]

The C_p at constant pressure is a temperature derivative of the enthalpy function [$C_p=(\Delta H/\Delta T)_p$], and thus, the enthalpy function can be measured through integration of the C_p [$H(T)=\int T/T0\ C_p(T)dT+H(T_0)$].[2]

ΔH, Change in Entropy (ΔS), ΔC_p of the T_m

For any biomolecule in aqueous solution, there would be equilibrium between the native conformation (folded) and its denatured state (unfolded). Stability of the native conformation is based on the extent of Gibbs free energy (ΔG) of the system and thermodynamic relationships between ΔH and ΔS.[39] A negative magnitude of ΔG represents higher stability of the native conformation than that of the denatured state. The more negative ΔG, the greater the stability. During the unfolding process of a protein, forces

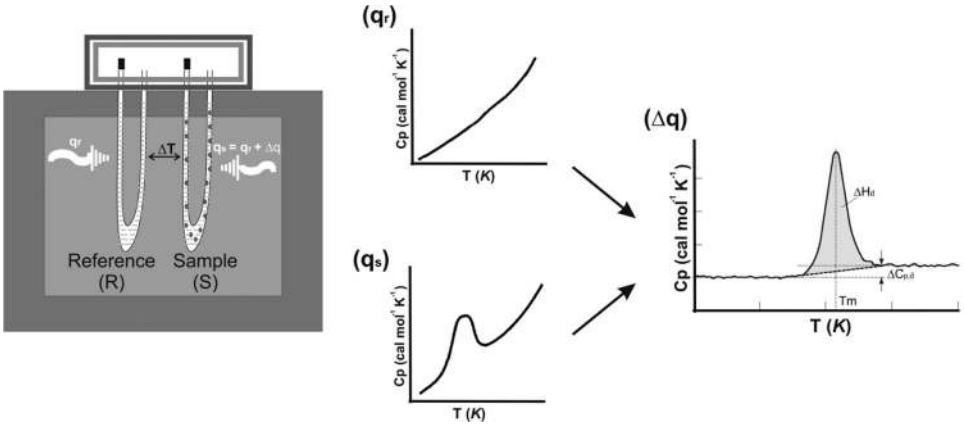

FIGURE 1

Experimental setup for a DSC experiment. The amount of heat required to increase the temperature by the same increment (ΔT) of a sample cell (qs) is higher than that required for the reference cell (qr) by the excess heat absorbed by the molecules in the sample (Δq). The resulting DSC scans with the reference subtracted from the sample show how this excess heat changes as a function of temperature.[33, 35] T (*K*), Temperature, kelvin; ΔH_d, change in enthalpy; $\Delta C_{p,d}$, change in C_p; T_m, transition and melting point; $_d$, denatured.

that play a key role in stabilization need to be broken. At temperatures where entropy is the dominant factor, conformational entropy overcomes the stabilizing forces, leading to unfolding of the protein.[40,41]

DSC measures ΔH of unfolding as a result of heat denaturation. The transition midpoint T_m is considered as the temperature, where 50% of the protein owns its native conformation, and the rest remains denatured. Higher T_m values would be representative of a more stable molecule. During the same experiment, DSC is also capable of measuring the ΔC_p. Associated with protein unfolding process, ΔC_p occurs as a result of changes in hydration of side-chains, which are buried in the native conformation but become exposed to the solvent in a denatured state.[40,41]

Calorimetric enthalpy (ΔH_{cal}) means the total integrated zone below the thermogram peak, which indicates total heat energy uptake by the sample after suitable baseline correction affecting the transition.[34]

van't Hoff enthalpy (ΔH_{VH}) is an independent measurement of the transitional enthalpy according to the model of the experiment.[34] ΔH_{VH} is determined through the shape analysis of an experimental graph of C_p^{ex} versus T.[42–44]

The state of the transition is evaluated by comparing ΔH_{VH} with ΔH_{cal}.[42,44] If ΔH_{VH} is equal to ΔH_{cal}, the transition occurs in a two-state mode. In such processes, meaningful thermodynamic results are determined through van't Hoff measurements of equilibrium results. When ΔH_{VH} is more than ΔH_{cal}, the intermolecular cooperation is shown, which is exposed, for example, as aggregation. Comparison between ΔH_{VH} and ΔH_{cal} also indicates the cooperative nature of the transition. Particularly, the $\Delta H_{VH}/\Delta H_{cal}$ ratio gives an estimation from the fraction of the structure, which is melted as a thermodynamical value. The value is also named as the size of the cooperative unit.[42]

C_p for the transitional state is obtained through the difference between pretransitional and post-transitional baselines of a DSC process.[34] The curve of C_p against T can be changed to C_p/T versus T through dividing the raw C_p value by T and drawing the results as a function of T. By integration, this curve results in the transition entropy (ΔS), which is expressed as $(\Delta S) = \int (C_p/T)\, dT$. Hence, an individual DSC thermogram can result in ΔH, ΔS, and ΔC_p.[42]

After knowing the above data, transition-free energy (ΔG) can be given at each temperature (T) through the thermodynamic equation $\Delta G = \Delta H - T\Delta S$.[42–44] Although ΔS and ΔG can be obtained by DSC results, the values are more unreliable than the ΔH and ΔC_p values determined directly because of coupling and propagating of errors.[42,45]

Absolute C_p

Apparent C_p can be obtained by DSC results. It includes the contribution of water displacement by the protein in the sample cell, which could have a negative value. Correction for the water displacement effect and normalization to a mole of protein offer the absolute C_p. The value is obtained from doing a series of DSC measurements at different protein concentrations.[46]

Determined absolute heat capacities by DSC could be used to characterize long-range interactions and cooperative phenomena, which have been shown to occur in denatured proteins.[47–49]

DSC APPLICATIONS IN BIOLOGY

Analysis of Proteins

It is well known that formation of unique structures of biological macromolecules, such as proteins and their specific complexes, is, in principle, reversible, and the reactions are thermodynamically driven. Therefore, thermodynamic investigations of these processes are of high priority. To achieve this goal, direct measurements of the heat effects associated with these intra- and intermacromolecular processes are required by the help of developed, supersensitive calorimetric techniques such as DSC,[50] which is considered one of the most frequently used techniques to determine thermal stability of proteins[51–61] and to measure the thermodynamic parameters of thermal protein unfolding.[31,51,62–64]

DSC offers a variety of applications in the evaluation of factors, which play the key role in protein stability. Therefore, it is possible to determine the most ideal conditions for stabilizing liquid formulations of proteins.[51,65] In DSC studies, the temperature at the maximum point of the C_p curve (T_m) represents the macromolecule stability.[51,53,62,66–70] There are several reports about the use of protein samples, which are reheated for evaluation of thermal reversibility of protein degradation.[51,53,68,70]

Through the first calorimetric studies of the temperature-induced unfolding of compact globular proteins, it has been noticed that the process is associated with extensive heat absorption over a temperature range, which depends on the solvent conditions, e.g., pH of the solution. Consequently, a significant C_p increment would be noticed.[50] Privalov et al.[50,71,72] showed that changing pH to higher values increases the stability of proteins, the heat effect of unfolding, and its sharpness (Fig. 2).

DSC, as a direct method, can also provide information about the real thermodynamic parameters of thermal transitions in proteins.[5,73,74] As one of the great advantages of DSC, it can detect fine-tuning of interactions between the individual domains of a protein. For instance, Makarov

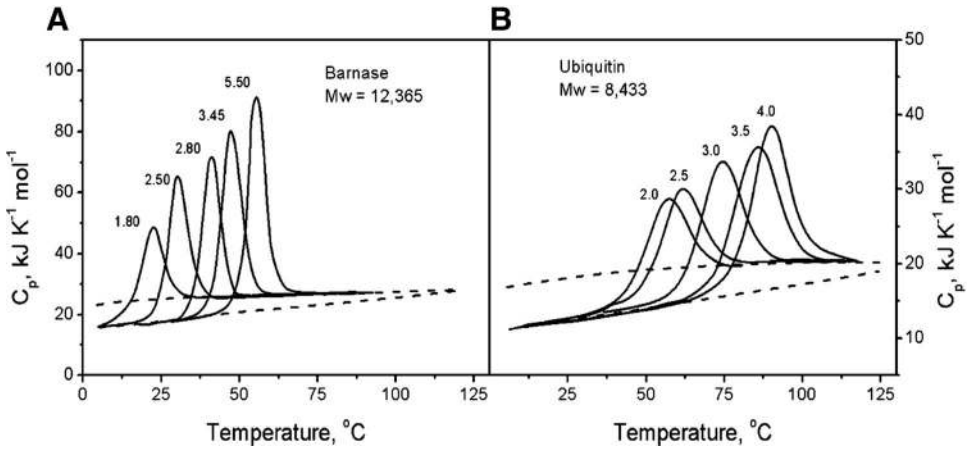

FIGURE 2

The partial molar C_p functions of (*A*) barnase (MW=12.4 kDa) and (*B*) ubiquitin (MW=8.4 kDa) in solutions with different pH. The dashed lines represent the partial molar C_p of native and unfolded proteins.[50]

and colleagues[5] analyzed the thermodynamic parameters of calcium ion-free synthetic calmodulin (apoSynCaM) and three charge-reversal mutants by DSC. They demonstrated that the heat denaturation of SynCaM8 and its mutants was estimated by two, two-state transitions, and the lower temperature transition was related to *C*-terminal lobe-melting and the higher temperature one to *N*-terminal lobe-melting. Also, they reported that the mutations modulate the thermodynamical parameters of SynCaM lobes in a similar mode, as pH conditions change thermal transition characteristics of multidomain proteins.[5]

Hydrophobic interactions and charged amino acid residues are considered to be important in the formation of calmodulin-peptide or calmodulin-drug complex formation.[5,75] Differences in thermodynamic parameters of denaturation for apoSynCaM and its mutants would be a reflection of the differences in their native states. DSC shows that transition parameters such as T_t and transition enthalpy (especially for the first transition) are quite different for SynCaM and its mutants. This confirms the key role of electrostatic interactions for stabilization of the native apoSynCam structure.[5] Makarov and colleagues[5] also reported that the values for denaturation enthalpy of apoSynCaM8 and apoSynCaM12A are near the corresponding values of apoSynCaM; whereas, in the case of apoSynCaM18A, they are lower, especially in 50 mM buffer. This demonstrates that the apoSynCaM18A molecule is less folded than others (Fig. 3).[5] With their calorimetric analysis, Makarov and colleagues[5] concluded that replacement of acidic clusters by basic ones in the SynCaM structure demonstrates the role of electrostatic interactions in the flexibility and stabilization of this protein.

DSC of Nucleic Acids

Application of calorimetric methods to study the thermodynamics of nucleic acid-folding transitions has gradually been improved in recent years. These improvements lead to the production of high-precision microcalorimeters. Hence, the amount of high-resolution structural results about nucleic acids has grown and clarified the physical–chemical interactions, which drive the formation of nucleic acid structures.[76]

DSC monitors the excess C_p of a nucleic acid in solution, and the temperature is increased or decreased with a constant rate (Fig. 4).[76] Measuring the differential heat flow between the sample and a reference accomplishes the excess C_p. When sample and reference are scanned simultaneously, folding and unfolding reactions occur in the nucleic acid as a consequence of absorbed or released heat. This differential heat is gained with subtraction from the reference thermal profile.[76,77]

Peaks obtained from types of DSC thermograms represent folding transitions, and melting points of the transition occur near the jump point of the curve.[76] The melting point (jump) corresponds to a single molecular transition, where ΔC_p is equal to zero. Integrating a peak or jump to temperature expresses the ΔH for the transition, and the corresponding ΔC_p can be obtained via the difference between pretransition and post-transition baselines.[2,77] ΔG and ΔS are also extracted through DSC results; however, the values are calculated indirectly and less reliably than DSC values. Melting points for short, double-stranded nucleic acids may need fitting to multiple transitions to account for a premelting transition, which has been correlated with opening and closing of the duplex.[77]

Peak results are fitted in such ways that accommodate limited ΔC_p or ignore them. The latter leads to ΔH_{VH}. The ratio of ΔH_{cal} to ΔH_{VH} could be used for study of intermediate folding states, which occur near the melting point.[42–44] Therefore, the DSC calorimeter is ideal for determining ΔC_p, measuring C_p directly.[76,78,79]

There are several important parameters in performing DSC on nucleic acids (DNA or RNA). The first is buffer; its acid dissociation constant value should not exhibit large temperature dependencies. Not only should a DSC buffer depend on its buffering capacity at a special pH, but also, it

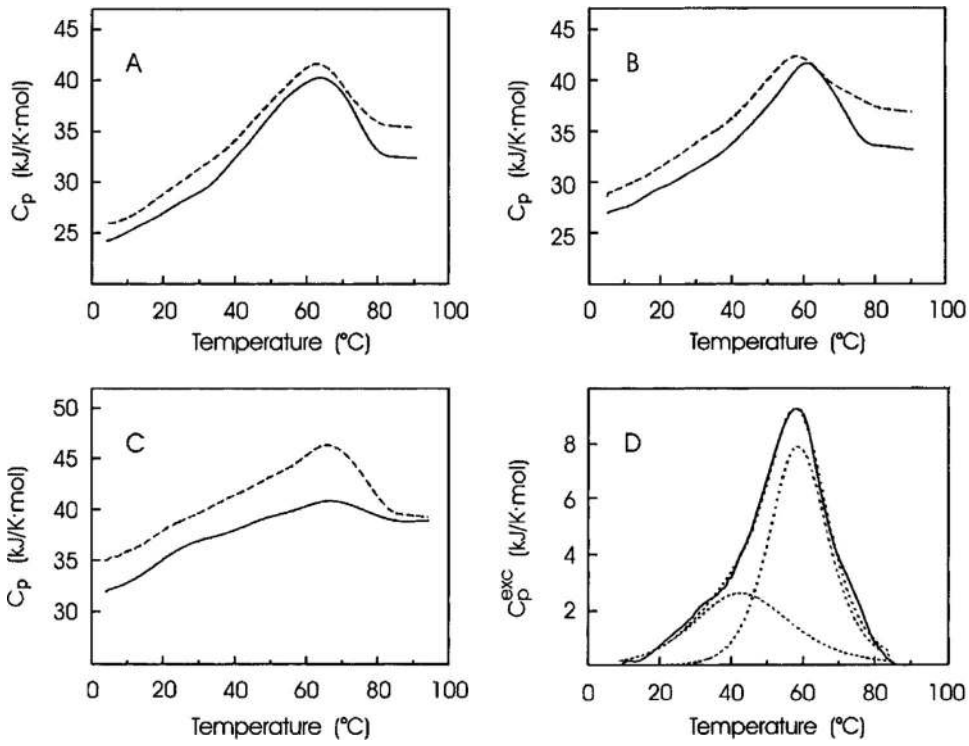

FIGURE 3

Temperature dependence of the partial molar C_p of apoSynCaM mutants in 10 mM (dotted line) and 50 mM (solid line) sodium cacodylate buffer at pH 7.5: apoSynCaM8 (*A*), apoSynCaM12A (*B*), and apoSynCaM18A (*C*). (*D*) Computer deconvolution of the transition excess C_p (C_p^{exc}) of apoSynCaM12A in 10 mM sodium cacodylate buffer at pH 7.5: experimental results (solid line), deconvoluted peaks, and their sum (dotted lines).[5]

should have minimal temperature dependence. Hence, the most-known buffers for DSC of nucleic acids contain phosphate, citrate, and acetate.[42] Second is the choice of salt or cation concentration in a DSC experiment. As the thermal stability of a polyanionic nucleic acid molecule depends on the concentration of salt in solution, a higher cation concentration leads to greater thermal stability of nucleic acids. The third important parameter in a DSC experiment is the concentration of nucleic acids. Enthalpy of a nucleic acid depends on its length and base sequence. Generally, the enthalpy decreases with shortening the fragment length. Hence, DSC of short nucleic acid fragments needs higher concentrations than those on long nucleic acids. Additionally, the minimum concentration of a given nucleic acid depends on the sensitivity of the calorimeter being used.[42]

In nucleic acids, the heat capacities of native and denatured states do not differ significantly, and in any case, the difference is not >0.06 Joules/Kelvin/gram ($JK^{-1}g^{-1}$).[80]

Analysis of Lipids

There are several reports about the use of DSC for analysis of oil and lipids. This class of macromolecules belongs to a vast number of molecules that merely share "a much better solubility in organic solvents than in water".[81–84]

The biomolecules offer a variety of functions, such as participation as structural components of biological membranes,[85–87] energy storage,[88] cell signaling,[89–93] cell growth and apoptosis,[94] transportation across membranes,[95–97] enzyme activation,[98,99] and others. Lipids, edible oils, and fats are abundant in many nutrition sources. Therefore, studies about autoxidation and oxidative stability of these food components are of high interest, as a result of having important economical, nutritional, and health values. For this purpose, conventional analytical methods are time- and solvent-consuming. Instrumental methods, such as electron spin resonance, IR, NMR, and chemiluminescence measurements, are sensitive to the noise and interferences that originate from autoxidation products and intermediates.[81] As heat is released in an autoxidation process, thermal analysis is a simple, direct, analytical method to follow the reaction by continuous monitoring of lipid oxidation and its thermal effects. Moreover, nonisothermal conditions of measurements (linear heating rate, β) offer the possibility of determining kinetic parameters much faster than the methods mentioned above.[81,100–104]

Litwinienko and co-workers[81] showed that DSC can be applied to study the oxidative stability of simple [linolenic acid (LNA)] and complex (lecithin) lipids. Comparison of the kinetics of soy lecithin autoxidation with that of LNA provides an opportunity to gain knowledge about the differences in thermoxidative behaviors of simple and complex lipids.[81] Fig. 5 shows typical DSC curves of nonisothermal oxidation of LNA for different heating rates.[81]

According to Ulkowski et al.,[81] DSC is a relatively fast analytical method for determination of oxidative stability. The kinetic parameters obtained by DSC allow the predic-

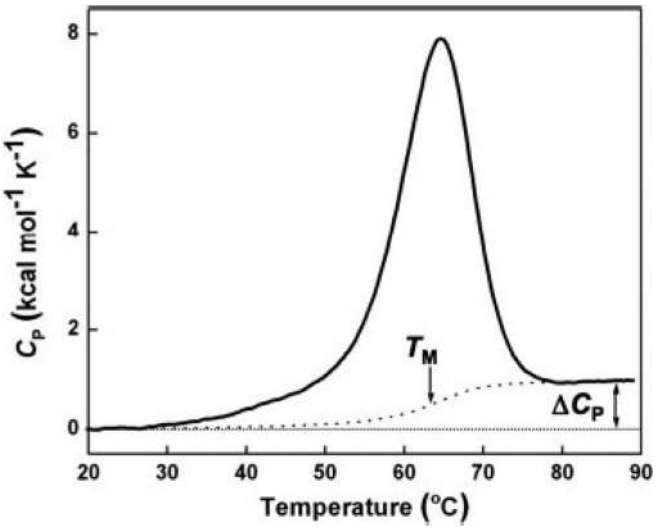

FIGURE 4

Example of DSC data for thermal melting of a 13-mer DNA duplex. The melting data (solid line) have been corrected by subtraction of a buffer blank data set and normalized for concentration of duplex. The calorimetric ΔH for the melting transition is obtained by integrating the area under the melting peak. The data can be fit to a thermodynamic model to extract the T_m and ΔC_p, as shown. ΔC_p, obtained from fits to DSC data and incur uncertainty as a result of the somewhat subjective process of assigning pre- and post-transition baselines.[76]

tion of oxidative behavior of lipids at lower temperatures, characteristic for the thermal conditions of food, fat storage, and handling. As an "ideal method", analytical signals of DSC can be connected directly with chemical changes occurring in the oxidized sample, without being misleading.[81]

Analysis of Carbohydrates

Starch granules, when subjected to heat treatment in the presence of water or other solvents, undergo a physicochemical transformation, famous as gelatinization.[105–110] Probing the physicochemical changes will contribute to better understanding of gelatinization processes. This phenomenon induces several changes in the starch granules, such as swelling, amylose exudation, loss of order, improved solubility and digestibility, granule disruption, and higher viscosity.[106,110–112] Many different measurement techniques have been reported for investigation of the starch gelatinization process.[106,108–115] Amongst all, DSC seems to be the most applicable technique, by which, the heat-flow changes associated with first- and second-order transitions of polymeric materials can be studied over a wide moisture and temperature range.[107,110,116–121]

Gelatinization in mixtures of sugars offers a promising frontier in clarifying the process, as mixing of sugars physically or naturally may provide novel formulations for a product with desired characteristics. From DSC studies, this process is considered as an endothermic process, involving two stages: cleavage of existing hydrogen bonds (endothermic) and formation of new bonds to give a less-ordered structure (exothermic).[110,115]

Sopade et al.[110] investigated the effect of glucose and fructose mixtures on starch gelatinization, using DSC. Concentrations of fructose and glucose were varied in the mixture of these monosaccharides at 0.86 g sugar/g dry starch in a starch-water system of 1 g water/g dry starch solution.

They also noticed that gelatinization temperatures of the fructose-glucose mixtures are not dependent on the mixture compositions, and the process occurs within the same range as for sole sugars. Fig. 6 indicates that for fructose-glucose mixtures, gelatinization proceeds in the same manner, as compared with each sugar alone, but at a slightly lower temperature with less energy.[110]

Reduction in the enthalpy of gelatinization (ΔH_{gel}) for lower temperature endotherm represents changes of thermal energy, which is required for the breakage and formation of hydrogen bonds within the starch granule. Furthermore, the resulting ΔH_{gel} from the mixture is compared with that of water. It seems fructose and glucose modify the characteristics of water, resulting in a higher ΔH_{gel}. This might be a result of the interactions between the two sugars, leaving the water chemically unaffected, thus having no effect on the amount of energy required for gelatinization.[110]

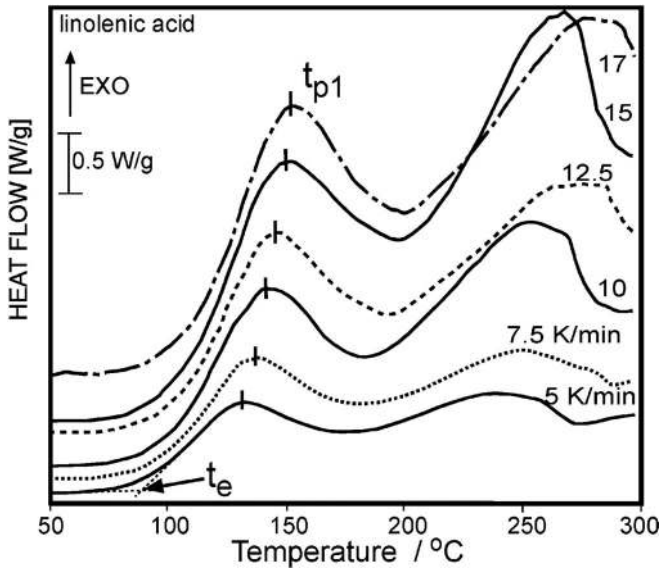

FIGURE 5

DSC curves of nonisothermal oxidation of LNA with a defined temperature of the extrapolated start of oxidation (t_e) and temperature of first peak (t_{p1}). EXO, Exothermic. Numbers denote heating rates in K/min.[81]

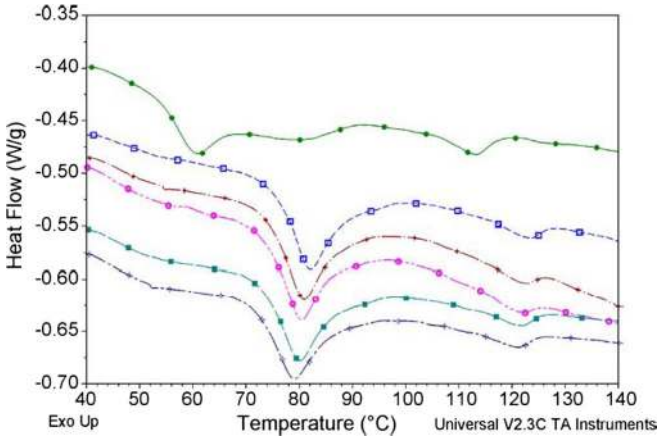

FIGURE 6

The gelatinization thermograms of the starch–fructose–glucose mixtures (from top/g dry starch; no sugars; 0.86 g glucose, 0.26 g fructose; 0.60 g glucose, 0.43 g fructose; 0.43 g glucose, 0.60 g fructose; 0.26 g glucose, 0.86 g fructose)[110]; TA Instruments (New Castle, DE, USA).

Fructose and glucose exhibit opposite behavior in the case of light polarization, and the influence of their chemical differences and opposite behavior (in mixtures) on the mechanism behind ΔH_{gel} has not been investigated so far. Sopade et al.[110] suggested that application of temperature-modulated DSC (MDSC), coupled with polarimetry studies, would be a good candidate for understanding the gelatinization process in sugar mixtures. This will also contribute to separation and better quantification of reversible and nonreversible reactions.[110]

Analysis of mAb

mAb have offered promising potential application as drugs in the pharmaceutical industry.[122] So far, >20 formulations have been approved, and hundreds more are under development.[122,123] Being a therapeutic agent, antibodies must be in the native, monomeric state to have a proper function with good stability.[124] It is also essential to minimize the aggregation of antibodies for pharmaceutical applications. They can be readily purified by conventional purification approaches, i.e., using affinity columns. The bound antibody is then eluted from the column at a low pH. Previously, it has been confirmed that at the time of purification and viral clearance, the acidic environment induces conformational changes in antibodies, particularly in their Fc domain.[124–132]

Hence, the importance of understanding such conformational changes, together with stability and aggregation of antibodies at different pH values, comes into the picture. Techniques such as near- and far-UV circular dichroism spectroscopy and sedimentation velocity can be used for this purpose.[124] Ejima et al.[124] studied the effect of acid exposure on the conformation, stability, and aggregation of humanized mAb (hIgG4-A). Using DSC, they evaluated thermal stability of the native hIgG4-A and the hIgG4-A samples at low pH.[124] Nano DSC thermogram revealed a biphasic thermal transition, which is typical for antibodies (Fig. 7).[124,133]

For the native form of hIgG4-A (pH 6), Ejima et al.[124] observed an endothermic P_{II} at 78°C and a P_I at 67°C, whereas at pH 3.5, the T_m of both peaks was shifted to lower temperatures, i.e., to 58°C for P_{II} and to 35°C for P_I. Such decrease in melting temperature of the antibody can be attributed to general pH-induced destabilization. Lowering of pH to 2.7 results in disappearance of the P_I, which is observed at pH 6.0 and pH 3.5. This might be a result of further destabilization of protein structure and conformational changes, particularly for the domain responsible for the P_I transition. Moreover, the P_{II} was split into two peaks, having T_m of 41°C and 46°C, which indicates further destabilization of the domain with higher stability.[124]

Ejima et al.[124] also noticed that the samples recovered from the DSC showed turbidity, consistent with irreversible thermal unfolding at pH 6.0 and pH 3.5, whereas at pH 2.7, the unfolding process was partially reversible with a transparent-recovered solution. The research group continued their DSC studies after storing the pH 3.5 sample at 4°C for 1, 3, and 10 days and the pH 2.7 sample at 4°C for 3, 6, and 10

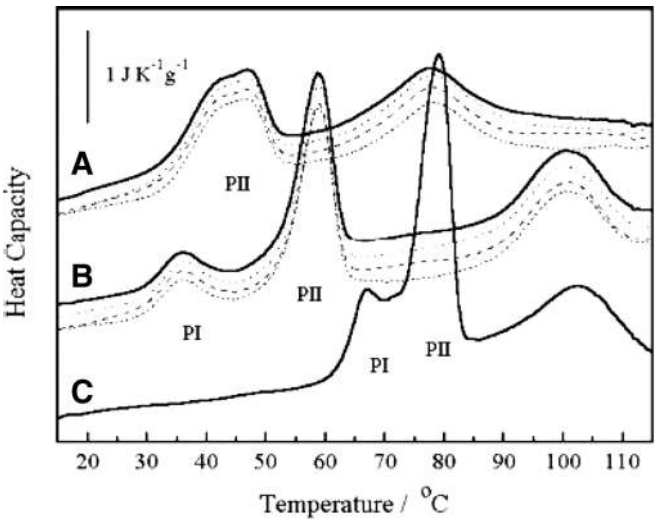

FIGURE 7

pH and time dependence of hIgG4-A C_p in 0.1 M citrate. hIgG4-A, adjusted to each pH by Protein A chromatography, was kept at 48°C for up to 10 days and measured by nano DSC. Calorimetry conditions are described in Materials and Methods. (*A*) At pH 2.7, immediately after elution (solid line, top), 3 days (dotted line), 6 days (dashed line), and 10 days (thin, dashed line, bottom). (*B*) At pH 3.5, immediately after elution (solid line, top), 1 day (dotted line), 3 days (dashed line), and 10 days (thin, dashed line, bottom). (*C*) At pH 6.0.[124] PI, Minor peak; PII, major peak.

days. Each scan was obtained immediately after elution, and DSC profiles were identical at each pH. Therefore, they concluded that when antibodies are stored at pH 3.5 or pH 2.7, no conformational change occurs over time.[124]

In another study, Protasevich et al.[134] used DSC to compare thermal denaturation parameters of Fab and $(Fc)_5$ fragments of native and rheumatoid IgM. They showed a thermodynamic similarity of $(Fc)_5$ fragments of both IgMs, and their Fab fragments had interaction differences between V_L-C_L and V_H-C_H domains. Hence, DSC could give important information about the thermodynamic characteristics of wild and disordered Igs to develop valuable approaches to diagnosis and treatment of some autoimmune diseases.[134]

DSC APPLICATIONS IN NANOSCIENCE

Quantification of Pharmaceutical Nanosolids

Regulatory aspects of the pharmaceutical nanosolids and an increasing number of insoluble molecules in the developmental pipeline have encouraged scientists for conducting further pharmaceutical researches and use of nanosolids.[135–137] Among various analytical techniques, DSC has been used for quantifying an amorphous or crystalline phase in nanosolids.[138] Several methodologies based on the calorimeter type (conventional DSC or MTDSC), measured parameters, and experimental conditions are used for monitoring the behavior of pharmaceutical nanosolids.[138–140]

Glass transition endotherm, crystallization exotherm, and fusion endotherm are the main parameters of an amorphous or crystalline material to be assessed while using conventional DSC.[138,139] Glass transition endotherm is a result of the presence of the amorphous phase, and the crystallization exotherm results from recrystallization of the amorphous content. Subsequently, the obtained crystalline state and the pre-existing crystalline content fuse together to form a melting endotherm.[138]

There are two approaches for determining the crystallinity percent of a sample via DSC.[138] The first one is carried out by calibration, using 100% amorphous and crystalline standards and physical mixing, which gives their corresponding heats of crystallization or enthalpies of fusion. Subsequently, the amorphous content of a certain sample can be assessed by its heat of crystallization or enthalpy of fusion through the following equation[138,141]:

$$X_c\ (\%) = \Delta H/\Delta H_0/100,$$

where, X_c is the percentage of crystallinity, ΔH is the enthalpy of fusion of the sample, and ΔH_0 is that of the 100% crystalline standard.[141] However, the following equation suggests another way to calculate the amorphous content with no need for preparing a calibration curve[138,142]:

$$\text{Amorphous content} = \Delta H_f^{amor}/\Delta H_f^{cry},$$

where ΔH_f^{amor} is enthalpy of fusion for the amorphous fraction, and ΔH_f^{cry} is the heat of fusion at the melting point for the purely crystalline material.[138,142] The amorphous content can also be obtained from the equation[138,143]:

$$T_{DSC} = \Delta H_{cr}(T_{cr})/\Delta H_m^0(T_{cr}) \times 1/1 - \alpha,$$

where T_{DSC} is the amorphous fraction of the sample, $\Delta H_{cr}(T_{cr})$ is the enthalpy of crystallization temperature, $\Delta H_m^0(T_{cr})$ is the enthalpy of melting for pure crystallinity at the crystallization temperature, and α is the percentage of the amorphous content that does not crystallize as a result of heating.[138,143]

The latter approach for determining the percentage of crystallinity by DSC is without preparing calibration standards, which includes subtracting the heat of crystallization from the heat of fusion. The result yields the heat as a result of the primary crystallinity of the sample, and the percentage can be calculated by the following equation[144,145]:

$$\%\text{Crystallinity} = \Delta H_f - \Delta H_c/\Delta H_{cry}^f \times m.$$

Here, ΔH_f is the fusion heat of the sample, ΔH_c is the heat of crystallization of the sample, ΔH_{cry}^f is the enthalpy of fusion of pure crystalline sample, and m is the sample mass.[138,144,145]

MTDSC can also be used for quantifying the amorphous content of a sample by the measurement of the C_p jump, which is corresponding to the amorphous phase glass transition. The value is obtained via the following equation and by preparing a calibration curve according to the C_p peaks of physical mixtures (PMs) of a known crystalline state (Fig. 8).[138,140]

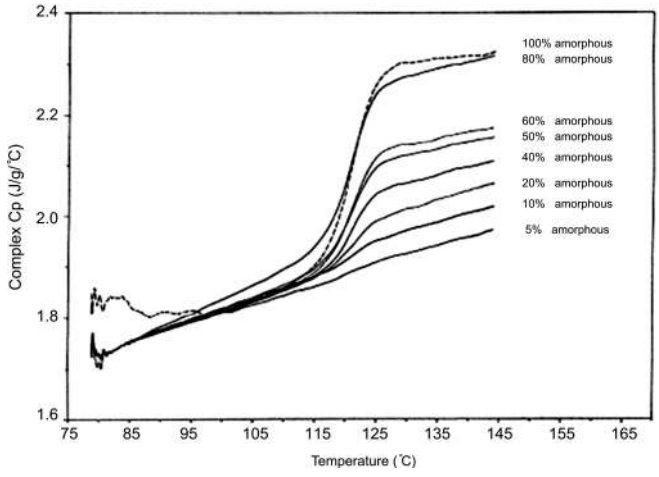

FIGURE 8

C_p jumps, recorded on various known mixtures of amorphous and crystalline forms of a developmental compound using MTDSC.[140]

$$C_p = K(C_p) \cdot Amp_{MHF}/Amp_{MHR}.$$

Here, $K(C_p)$ is the C_p constant, and Amp_{MHF} and Amp_{MHR} are the amplitudes of modulated heat flow and modulated heat rate, respectively.[138,140] Alternatively, several parameters, such as thickness of the sample bed in the pan, thermal contact resistance between the sample and the pan, and thermal contact resistance between the sample and the base plate of the system, could be considered for a more precise measurement of the C_p.[138,146]

Recently, various reports have addressed the use of MTDSC for characterization of drug-loaded nanosolids.[147–149] For instance, Yu et al.[149] demonstrated that ibuprofen is dispersed in PVP K30 fibers in the form of nanosolid dispersing, with an amorphous physical state based on its content in the nanofibers (Fig. 9). Additionally, it was shown that ibuprofen molecules serve as a plasticizer for the nanofibers, leading to a reduction in their T_g.[149]

Thermal Characteristics of Nanostructured Lipid Carriers (NLCs)

Lipid nanospheres are considered as drug delivery carriers. Having potential application in medicine, these nanoparticles have been used extensively during the recent years. Lipid nanospheres offer a variety of advantages, including enhancement of the therapeutic effect,[150] biodegradability,[151] good tolerability,[152] bioavailability in case of ocular administration,[153] and capability of brain targeting.[154,155]

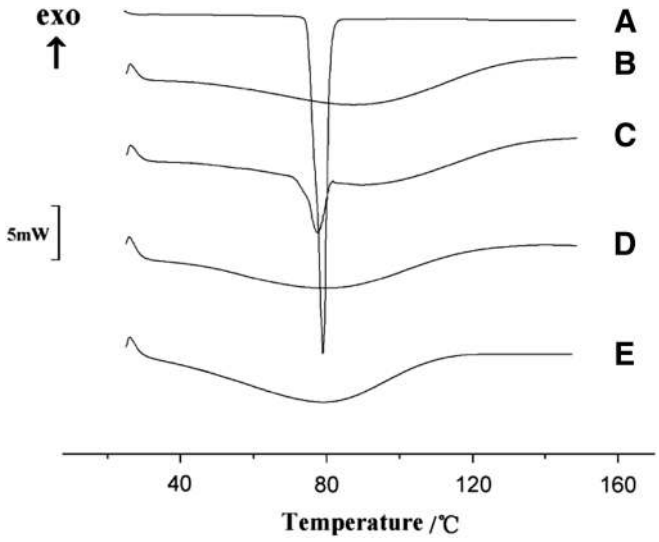

FIGURE 9

DSC curves: (*A*) ibuprofen, (*B*) PVP, (*C*) PM of drug and PVP, (*D*) F1 fibers, (*E*) F2 fibers. DSC thermogram of pure ibuprofen exhibited a single endothermic response corresponding to the melting of the ibuprofen at 77.5°C. As an amorphous polymer, PVP K30 did not show any fusion peak or phase transition, apart from a broad endotherm, as a result of dehydration, which lies between 80°C and 120°C. DSC curves of F1 fibers and F2 fibers (*D* and *E*) did not show any melting peak of the drug but a broad endotherm ranging from 70°C to 110°C with the glass T_t (T_g) of F1 fibers higher than that of F2 fibers. For the PM, the endotherm broadened and was shifted slightly to a lower temperature (76.8°C), reflecting a partial change of ibuprofen crystal structure.[149]

Solid lipid nanoparticles (SLNs) and NLCs can be categorized as two main types of lipid nanospheres.[155] SLNs introduce a variety of advantages, such as controlled drug delivery, development of emulsion, liposomes, and fine particles,[156] protection of active ingredients against degradation by chemicals, and incorporating a high degree of flexibility in the modulation of the drug release profiles. Apart from all, it is possible to produce SNLs in an industrial large scale by high-pressure homogenization.[157,158] However, there exist some limitations while using SNLs, i.e., low drug entrapment efficiency (EE) and drug expulsion.[155,156]

To overcome the limitations mentioned above, Yuan and co-workers[155] developed a solvent diffusion method in a drug-saturated system and investigated the efficiency of drug encapsulation into lipid nanospheres by the help of DSC. NLC, with its solid lipid matrix, is composed of certain liquid lipid content [i.e., caprylic/capric triglycerides (CT)]; therefore, it might be addressed as a new generation of lipid nanoparticles. Incorporating liquid lipids into a solid matrix will create some imperfections in the crystal lattice of nanoparticles. The greater imperfections in the lattice structure, the more reduction in drug repulsion (during the storage) and higher drug-loading capacity.[155,159–161]

Yuan and colleages[155] compared the drug EE of lipid nanospheres by two methods: conventional solvent diffusion and solvent diffusion in a drug-saturated aqueous system. They used nimodipine as a model drug for incorporation into lipid nanospheres and investigated whether the drug-loading capacity could be enhanced with DSC studies. Fig. 10 shows the DSC curves of NLC and compares two methods of conventional solvent diffusion and solvent diffusion in a drug-saturated aqueous system, before and after washing with 0.2% SDS solutions. For monostearin (MS) SNLs, the melting temperature is 56–58°C, whereas it comes to 124–128°C for the model drug (nimodipine). Therefore, any peak between 50°C and 60°C in DSC curves would be corresponding to the mixed lipid matrix of MS and CT, and nimodipine can be identified by its DSC peak position near 90°C. As shown in Fig. 10, DSC analysis is done for NLC, prepared by both techniques, before and after washing with 0.2% weight SDS solution.[155]

Comparison of the curves A and C with curves B and D indicates the appearance of the nimodipine peak before washing with SDS solution, and this peak disappears after the washing treatment. This is a result of the presence of nimodipine on the surface of the lipid nanoparticles, which is

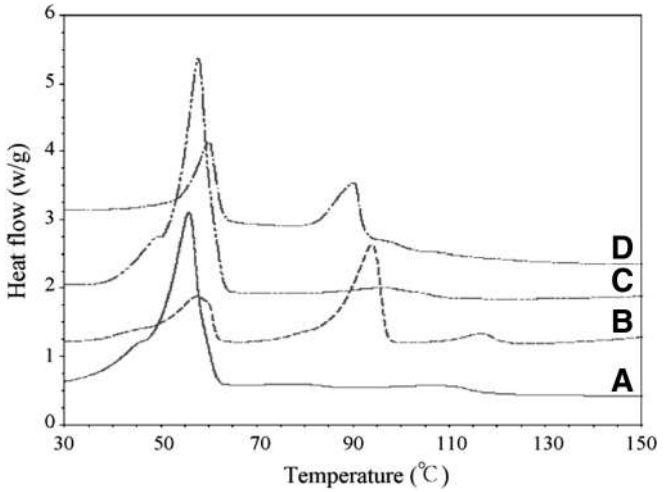

FIGURE 10

DSC curves of NLCs. (*A*) NLC prepared by the conventional solvent diffusion method after washing with 0.2 weight percent SDS solution; (*B*) NLC prepared by the conventional solvent diffusion method before washing with 0.2 weight percent SDS solution; (*C*) NLC prepared by the solvent diffusion method in a drug-saturated aqueous system after washing with 0.2 weight percent SDS solution; (*D*) NLC prepared by the solvent diffusion method in a drug-saturated aqueous system before washing with 0.2 weight percent SDS solution.[155]

washed away after using SDS solution. Hence, the peak for nimodipine vanishes.[155]

A glance at curves B and D shows that the peak area ratio of nimodipine-to-lipid matrix for curve D is lower than that of curve B. From the DSC graph, Yuan and co-workers[155] concluded that the lower peak area ratio is a result of the reduction of nimodipine content on the surface of NLC. Thus, the drug EE of NLC is improved significantly by using the second method, i.e., solvent diffusion in a drug-saturated system.[155]

Thermoanalysis of Colloidal Nanoparticles

Colloidal nanoparticles are classified as inorganic nanoparticles, organic nanoparticles, and organic/inorganic composite nanoparticles that could be used in nanobiotechnologies.[162] Inorganic nanoparticles generally include gold nanoparticles,[163] metal oxides (such as ferrofluids, super paramagnetic particles),[164] other metallic and bimetallic nanoparticles (such as Pt, Pd, and Ru),[165] silica nanotubes,[166] and semiconductor nanocrystals (quantum dots),[167] which have known applications in colorimetric detection of DNA sequences,[168,169] medical imaging,[170] labeling for chip-based DNA detection,[171] biological sensing,[172] and quantification of biomolecules.[173]

The best-known organic nanoparticles include carbon nanotubes and fullerenes,[174] dendrimers,[175] polyelectrolyte complexes in natural or synthetic forms,[176] self-assembled block copolymers of polyethylene oxide,[177] SLNs,[178] and latexes.[179] There are various reports about their applications in DNA targeting,[180] reservoirs of drugs,[181] drug targeting and vaccination,[182,183] drug delivery systems,[184,185] solid-phase assays, and two-dimensional arrays.[186,187]

Organic or inorganic composite nanoparticles are categorized in magnetic nanoparticles,[188] fluorescent nanoparticles,[189] silica-based nanoparticles,[190] and polymer-metal nanocomposites (e.g., gold and polypyrrol),[191] which commonly have been used in diagnostics,[192] extraction of DNA, cells, and viruses,[193] time-resolved fluorescence assay,[194] and special bioanalyses[195] and bioassays.[196]

There are various analytical techniques for physicochemical analysis of colloidal nanoparticles.[197,198] One of these techniques is DSC, which could be used for stability measurements.[197] For example, thermal analysis of the SLNs by DSC gives important information about the crystallization behavior, the timing of polymorphic transitions, the fusion melting, the enthalpy, and the crystallinity percentage of melt-homogenized glyceride nanoparticle dispersions.[199,200]

In another study, Hui et al.[181] have used DSC for thermal analysis of dendrimer derivatives polyamidoamine-g-poly(*N*,*N*-dimethylaminoethyl methacrylate) (PAMAM-g-PDMA), while feeding with different ratios of DMA components (Fig. 11) The thermograms show that T_g gradually decreases as a result of the increase in the feed ratio, and subsequently, the increasing feed ratio can lead to a longer graft chain on the surface of dendrimers. Hence, the longer graft in polymers results in a lower T_g in practice.[181]

Glass Transition Measurement of Macromolecules in Nanophases

Thermodynamically, a phase is defined as the physical state of matter, which is uniform throughout.[201] Differ-

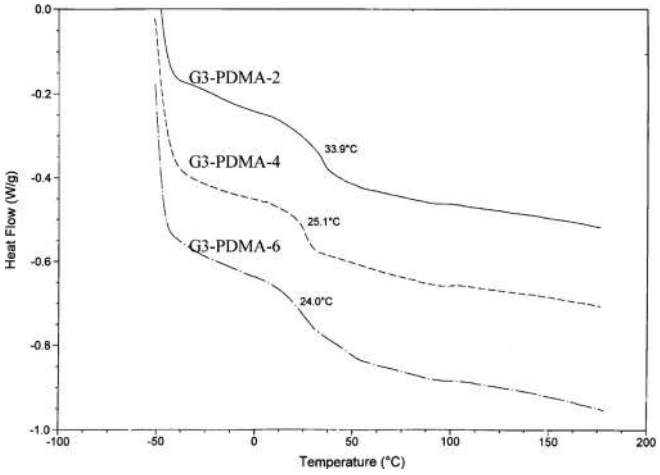

FIGURE 11

DSC thermograms of dendrimer derivatives PAMAM-g-PDMA.[181]

ent phases are considered as domains that differ in chemical or physical states. According to the size, phases are classified as macrophases (i.e., bulk phase), microphases (i.e., small phase with strong surface effects), and nanophases (1–50 nm).[201,202] There are various experiments supporting the fact that macrophases have only negligible surface effects and are usually limited in size to dimensions larger than 1 μm.[201–204] Microphases are affected in their properties by the surface, as indicated by the Gibbs-Thomson equation for the melting of thin, lamellar crystals.[202] Microphases still have a bulk phase in the center of their volume. The nanophases contain no bulk phase at all, and their surface may cause a decrease in T_g when the mobility increases at the interface.[202] Also, the surface may contribute to an increase in T_g when there is a stress transfer at the interface, as in the rigid amorphous fraction (RAF).[202] Hence, the upper limit of size of a nanophase is different for the different phase structures.[201,202] For measuring the change of heat C_p of various macromolecules (e.g., polymers) in the glass transition region, DSC could be used.[205,206] Nanophase is the lower limit of the usefulness of a thermodynamic phase description because of atomic contents of matter, and hence, the surface effects change the characteristics of the phase significantly.[201,202]

T_g is one of the important thermodynamical parameter changes in nanophases of matter, and it is practically measurable using DSC.[201–203] Glass transitions are also defined as "brittle points" to mark a transition from the liquid to the solid state.[202] For instance, the value changes in small spheres of polystyrene in nanophase dimensions in

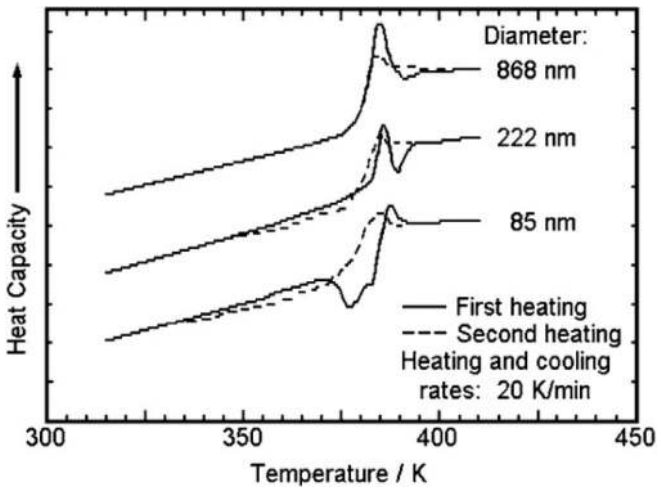

FIGURE 12

Change of the glass transition of polystyrene with decreasing size of the phase.[201]

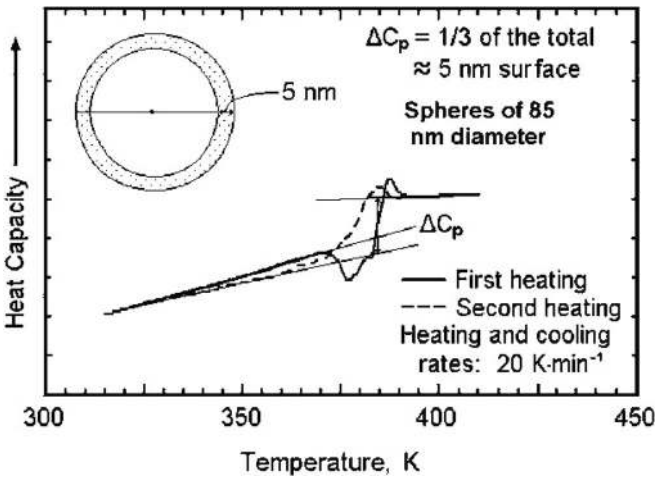

FIGURE 13

Calculation of the surface volume of poly(styrene) to assess the lowering of the glass transition at the surface of small spheres based on DSC measurements. Note the ~50 K shift of the beginning of the glass transition when going from the solid to the dashed line.[202]

comparison with the other phases of matter when measured by DSC (Fig. 12).[201,203]

As illustrated by Gaur and Wunderlich[203] about first heating, the beginning of T_g in small spheres occurs at a lower temperature, and the midpoint of C_p jump indicates minute changes. This occurs lower than the beginning of the T_g for the smallest spheres.[201,203] The study shows the dependency of glass transitions to size and surface of phases.[201] In addition, Gaur and Wunderlich[203] explained about the dividing line between the micro- and nanophases, as illustrated in Fig. 13.[202] The broadening of glass transition by nearly 50 K is interpreted as caused by increased mobility at the surface. By matching the heat capacities, the surface layer is about 5 nm thick, which in turn, suggests that a sphere with a radius of 5 nm would only be surface material and contains no bulk phase.[202,203] The RAF in the semi-crystalline polymers is then expressed as a nanophase of characteristics in comparison with the bulk amorphous phase.[202,203]

Characterization of Ion-Chelating Nanocarriers

Chitosan is one polysaccharide-based nanocarrier,[207] whose major application is based on its ability to entrap strongly heavy and toxic metal ions (such as Cu, Co, Ni, Cd, Zn, Pb, Mn, Cr, Pd, Pt, Au, Ag, Hg, U, Ga, and In).[208–210] Hence, one of the excellent applications of these nanoparticles is for removing metallic impurities in wastewaters.[211] In addition, chitosan, as a natural polymer, has potential applications in biomedical products, cosmetics, and food processing.[212]

As reported, the polymer has the highest chelating capability in comparison with other natural and synthetic polymers that have been used in commercial chelating

ion-exchange resins.[213,214] The binding capacity has been estimated >1 mmol/g for heavy and toxic metals.[211]

The mechanism of the sorption can be determined using various kinds of analytical techniques including DSC. Importantly, DSC is an effective device for characterization of chitosan and its metal chelates.[211] Generally, the DSC curve of chitosan–metal chelates indicates two peaks: the endothermic peak (at 100°C) and the exothermic peak (at 310°C) (Fig. 14).[215,216] T_g of chitosan was seen at 203°C.[216] The causes of the peaks include the vaporization of water in the substance and the oxidative degradation and deacetylation.[211,216]

In the other experiments, mercury ion (Hg^{2+}), copper ion (Cu^{2+}), and ferric iron ion complexes of chitosan have been characterized using DSC.[217] The results indicated that there was a minute elevation above the chitosan in the decomposition temperature of the metal complexes.[217] The phenomenon was considered to be a result of two opposing factors. The first factor is the conformational changes of chitosan leading to thermal instability.[211] The other is an additional bridging through the metal ion leading to enhanced thermal stability.[211] An additional observation was that the Hg^{2+} complex indicated three endothermic T_t at 206°C, 220°C, and 242°C.[211] However, the Cu^{2+} complex demonstrated a single peak at 203°C, which may be a result of a new crystalline-phase formation.[211]

Self-Assembly Study of Supramolecular Nanostructures

The self-assembly phenomenon is a bottom-up approach (e.g., in nanoscience) to make supramolecular nanostructures function appropriately.[218] The concept is based on chemical, physical, and biological characteristics of molecules to hold together and provide noncovalent intermolecular-binding interactions.[219] The main noncovalent

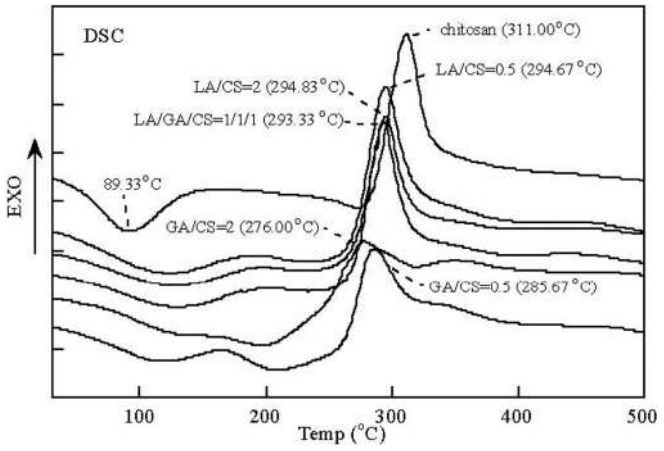

FIGURE 14

DSC thermograms of chitosan and its derivatives.[216] LA, Lactic acid; CS, water-soluable chitosan; GA, glycolic acid.

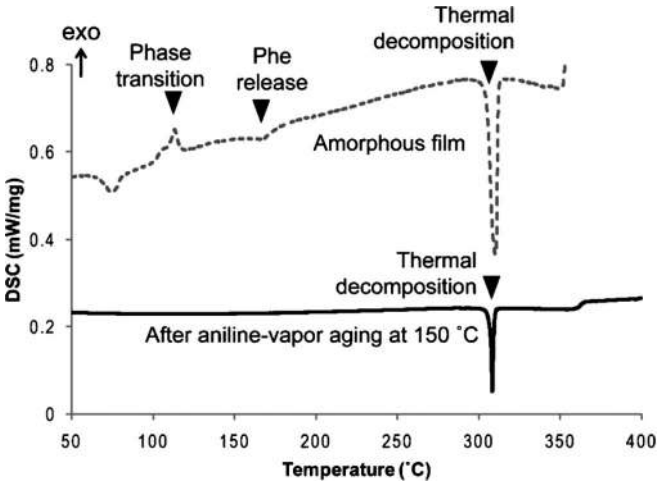

FIGURE 15

Thermal analysis of amorphous diphenylalanine films before and after high-temperature aniline vapor-aging at 150°C. Amorphous and nanowire films were characterized by DSC.[226]

forces of self-assembly are van der Waals interactions, electrostatic interactions, hydrogen binding, and molecular complementary.[220] The interactions have important roles in biomolecular systems (such as DNA, RNA, proteins, lipids, pharmaceuticals, nanostructures, etc.) to form and do their functions properly.[221,222]

There are various techniques to use for investigation of the self-assemblies.[198,223] DSC, as a thermal analytical tool, is carried out to gather more information about the self-assembly behavior of the suprastructures.[224,225] For example, Ryu and Park[226] investigated the thermal characteristics of the amorphous peptide film and the peptide nanowires (one of the solution-based approaches to peptide nanofabrication), grown through high-temperature aniline vapor-aging, by using DSC (Fig. 15).

The thermogram indicates a thermal decomposition of diphenylalanine completed at 308°C.[226] Endothermic and exothermic peaks of the amorphous diphenylalanine were seen at 175°C and 115°C, respectively.[226] The peaks were a result of the release of phenylalanine from diphenylalanine and phase transition, respectively.[226] In addition, the obtained results confirmed that the peptide nanowires formed through high-temperature aniline aging, meaning no phase-transitional behavior existed.[226] Also, it seemed that a negligible weight change occurred upon heating to 200°C, and scanning electron microscopy showed no structural changing in the nanowires upon heating to that temperature too.[226]

In another study, comparative structural and retrostructural analysis of the dendritic peptides (as natural porous proteins[227–233]), self-assembled from the complexes of achiral dendritic alcohols[234,235] and dendritic

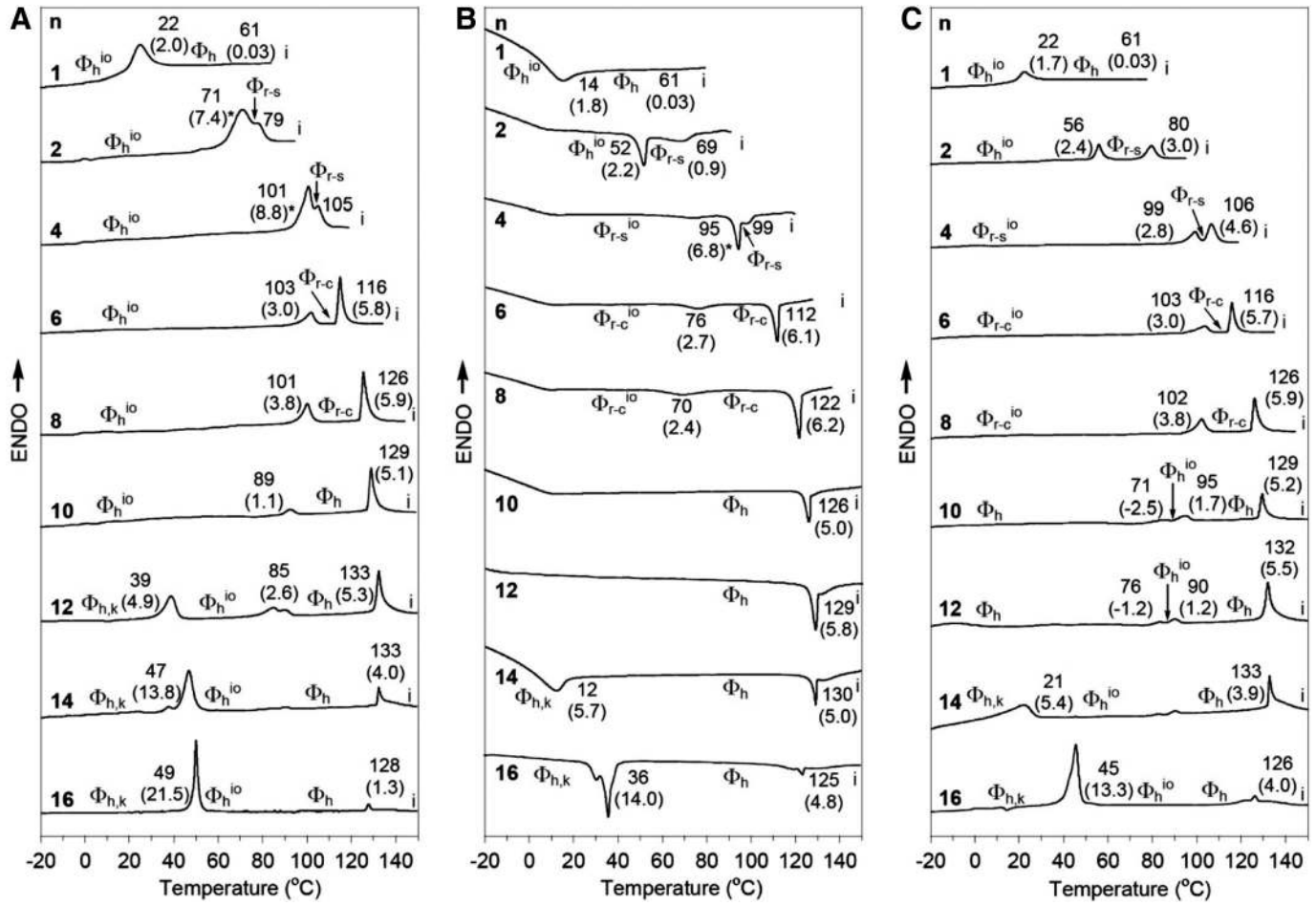

FIGURE 16

DSC traces of (4-3,4-3,5)nG2-CH2OH. T_t (°C) and enthalpy changes (kcal/mol, in parentheses) are marked on DSC. (*A*) First heating scan. (*B*) First cooling scan. (*C*) Second heating scan. *Sum of enthalpy changes for two overlapped peaks. i, Isotropic.[236] ENDO, Endothermic.

dipeptides,[234] has been performed using solid-state techniques such as DSC (Figs. 16 and 17).[236]

The thermograms indicated that all solid samples are already self-assembled into supramolecular columns that have a circular cross-section in the case of various hexagonal columnar lattices (Φ_h) or in a slightly distorted, avoidable situation, in their rectangular columnar lattices (Φ_r).[236] In addition, during the first DSC scan, the dendritic alcohols with $n = 4$, 6, and 8 self-assemble into circular columns that self-organize into Φ_h phases. These columns become slightly distorted during subsequent heating and cooling scans and therefore, self-organization Φ_r^{io} phases.[236,237] During the first heating scan, the dendritic dipeptides with $n = 1$, 2, and 4 form Φ_r^{io} phases, whereas during the second scan, they produce glassy, amorphous solids. It was also determined that the dendritic alcohols with $n = 1$ and 2 provide cases of nonamphiphilic dendrons that self-assemble into supramolecular columns.[236,237]

DSC TECHNIQUES

MEMS-DSC

MEMS is a method applied in manufacturing three-dimensional silicon-based structures with specific geometrical, mechanical, and electrical characteristics to operate certain functions.[238] The idea of MEMS-DSCs was formed as a result of two functional problems of conventional DSCs, which prevent them from performing effectively in biomolecular structural transitions.[239] The problems could be summarized as: inadequate sensitivities[15,239] and use of external heaters to control the device chamber temperatures.[240,241]

MEMS-DSC is a polymer-based and miniaturized DSC with integrated microfluidics for analyzing structural transitions of biological molecules in liquid phase.[15,238] MEMS-DSC contains all of the essential components, including a heating resistor, a temperature sensor, a sensor to determine temperature differences, a well-defined thermal conductance, and a container.[237]

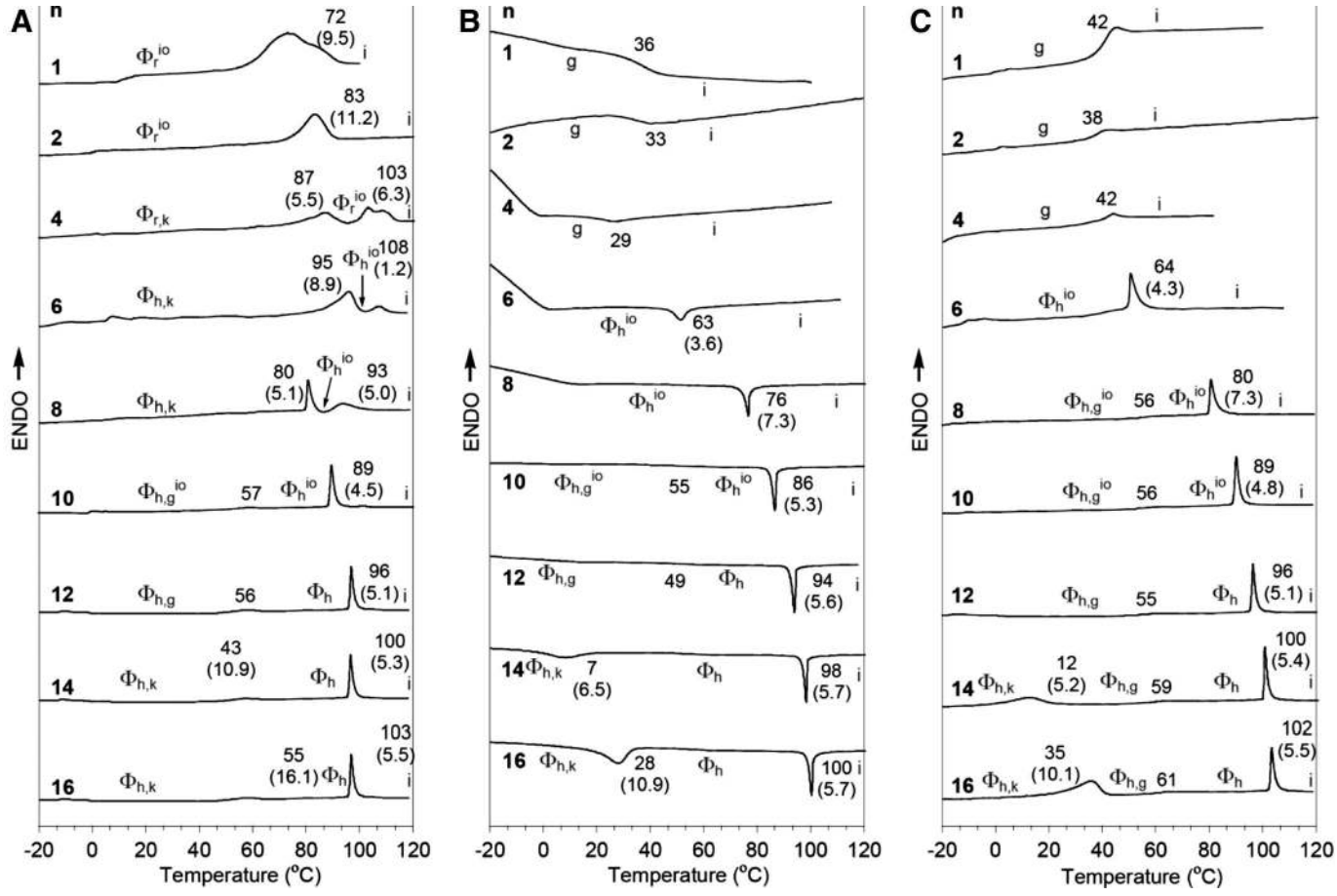

FIGURE 17

DSC traces of (4-3,4-3,5)nG2-CH_2-Boc-L-Tyr-L-Ala. T_t (°C) and enthalpy changes (kcal/mol, in parentheses) are marked on DSC. (*A*) First heating scan. (*B*) First cooling scan. (*C*) Second heating scan. g, Glass.[236]

MEMS-DSC contains two microfluidics chambers, which have their respective inlets and outlets connected through microchannels.[15,238] Each chamber is embedded by an air space for maximum thermal isolation and minimum thermal mass. In addition, each chamber contains a polymeric membrane, which with the microfluidic channels and chambers allow efficient handling and measurements of 1 μl samples.[238]

One thermopile is integrated with its hot and cold junctions (formed between Ni and Cr) on the membranes in the sample and reference chambers. Hence, using a low-noise thermopile temperature sensor and optimized thermal structures, sensitivity at approximately 50 nW could be obtained.[15,238] Also, a resistive temperature sensor and heater exist on each membrane to make a temperature control on the silicon chip. The resistive heaters and temperature sensors allow varying temperatures with prescribed rates. An island from Cu is enclosed to the backside of the membranes to extend their temperature uniformity.[15,238]

For analysis, one chamber is filled with a sample and the other with a reference buffer. Temperatures of sample and buffer are controlled in a closed loop by the sensors and heaters. Minimum differences of the temperatures between the sample and buffer are measured by the thermopile.[15,238] Any difference in the temperatures reflects structural changes of the sample and is used to assess the thermodynamic characteristics of the molecules.

The most known applications of MEMS-DSC have been reported for measurement of protein denaturations, yielding melting points in agreement with the literature values by basic DSCs.[239,240] For instance, Wang et al.[241] applied this system to measure thermodynamic parameters of lysozyme when thermally unfolded. As their MEMS calorimeter was equipped with a thermopile device, they could also monitor the thermal activity of the protein by thermopile output voltage. This capability leads to computation of differential C_p versus scanned temperatures. The obtained result (T_m~68.1°C) was in excellent agreement with the literature value (T_m~66.2°C),[31] and the calorimeter showed that it can indeed be applied for structural transitions of biomacromolecules in liquid.[240]

IR-Heated DSC

IR-heated DSC is a heat-flux DSC, which is comprised of a DSC sensor assembly for receiving a sample that is installed in a cavity within an elongated cylinder and an IR lamp assembly disposed of circumferentially around the elongated cylinder having a length substantially similar to that of the cylinder.[242] The measurement assembly comprises an elongated, high thermal conductivity cylinder having a cavity in which the DSC sensing assembly is situated and a high emissivity outer surface.[242] The IR lamp assembly preferably comprises a plurality of tubular lamps, each having a longitudinal axis arranged parallel to the axis of the elongated cylinder and an IR reflector comprising a plurality of partial cylindrical surfaces, which each describes as a cylindrical shape with a focus collinear with the axis of each tubular lamp.[242,243] The IR furnace is used to heat a measuring assembly that incorporates a high thermal conductivity enclosure similar to that of a conventional DSC.[242] The enclosure reduces temperature difference errors that result from heat exchange among the sensor, sample pans, and their surroundings. Given the size of the enclosure, much more IR energy from the lamps must be delivered to the measuring assembly to achieve a desired heating rate, and more energy must be removed to achieve a desired cooling rate.[242]

The calorimeter further comprises a thermal resistor coupled to the measurement assembly, wherein the thermal resistor is disposed of substantially outside of a region whose perimeter is defined by a cavity within the lamp assembly and a heat sink thermally coupled to the thermal resistor and to the IR reflector.[16,242] The heat-flux DSC includes a single thermal resistor used to thermally connect the measuring assembly to the external heat sink located externally to the reflector.[16,242] The thermal resistor is also located externally to the reflector, wherein the resistor is disposed of outside of the region defined by the reflector cavity.[16,242] The thermal resistor may be comprised of a solid material having the requisite composition and geometry to create the desired heat-flow restriction, or it may be a small gap filled with gas, such that the gas thermal conductivity and the gap dimension create the desired heat-flow restriction.[16,242] When the thermal resistor comprises a gas-filled gap, the gas composition may be changed to modify the magnitude of its thermal resistance. Rather than using a separate cooling system for the reflector, it is also coupled to the heat sink so that it too is cooled by the heat sink.[16,242] In this manner, the cooling rates and the minimum temperature achieved by the apparatus are improved. In addition, the device is simplified by elimination of a separate cooling system for the IR reflector.[16,242]

The exterior surface of the DSC enclosure that surrounds a measurement assembly is an elongated circular cylinder that is approximately equal in length to a reflector cavity and lamp assembly that forms an IR heating assembly.[16,242] In this manner, the DSC enclosure intercepts a greater fraction of the energy emitted by the lamps and reflected by the reflector.[16,242]

The DSC enclosure comprises a high emissivity exterior surface and a single high emissivity material.[16,242] It comprises an enclosure, such as a cylindrical enclosure, whose emissivity is not high in an inner portion of the cylinder walls but whose exterior surface is coated or laminated with a high emissivity layer to greatly increase the absorption of radiation arriving at the surface. In addition, in embodiments of the device, the measuring assembly is constructed without a surrounding quartz tube, which is conventionally used to enclose the measuring assembly.[16,242] This further improves heat-exchange efficiency and also allows the lamps to be positioned closer to the measuring assembly, which in turn, allows the reflector surface area to be reduced. The ratio of heated area to reflector area is thus increased, further improving the efficiency of IR heating.[16,242]

A single heat sink is used in the DSC apparatus and is located externally to the IR furnace reflector so that the heat sink is not heated directly by radiation, still further improving the efficiency of IR heating.[242] The heat sink may be cooled by circulating water or some other fluid as a coolant. Alternatively, the heat sink may be cooled by evaporation of a subcooled liquid, which may be the refrigerant in a vapor compression refrigeration system or an expendable coolant, such as liquid nitrogen, whose vapor is discharged to the atmosphere.[16]

IR-heated DSC is also named as rapid-heating DSC (RHDSC).[244,245] The calorimeter can offer heating rates up to 2000°C min^{-1}, providing a new opportunity to characterize unstable polymorphs as a result of the likelihood that form changes can be inhibited at higher heating rates. Hence, Gaisford et al.[245] used RHDSC to isolate and characterize paracetamol form III. In fact, they could isolate paracetamol form III from the glass and then quantify its melting point by heating it fast enough to inhibit the solid-solid transition to form II. This was achieved using heating rates more than 400°C min^{-1}.[245]

In summary, this type of DSC is configured to provide more rapid sample heating and cooling rates in comparison with conventional systems. Additionally, configurations of the system provide a more efficient arrangement for heating a DSC when the heat source is a plurality of lamps emitting IR radiation.[16,242] More versatile sample measurements are provided by embodiments in which a heat-flux DSC includes a configurable thermal resistor.[16,242,243] Thus, the thermal conductivity of the thermal resistor can be decreased during sam-

ple heating and increased during sample cooling, which allows the sample heating rate and sample cooling rate to be maximized independently during a single experiment.[16,242,243]

MTDSC

MTDSC provides the amplitude and phase signals [alternating current (AC) signals] and the total heat-flow signal equivalent to that given by DSC simultaneously in a single experiment.[11,246–249] The name MTDSC was copyrighted by TA Instruments.[17] The technique used a conventional DSC, and the signals were produced by a deconvolution procedure carried out by a computer.[17] A sinusoidal temperature modulation is the program used most often; however, there are many different forms of temperature programs for this aim.[17]

In addition to the technique, a simple theory and method of interpretation were introduced that focused on the differences between the AC and nonreversing signals [direct current (DC) signals].[17] Briefly, MTDSC is an advanced technique, in which the total heat-flow signal is obtained as the temperature of the sample, and reference is heated according to a basic heating rate, upon which, a temperature oscillation has been superimposed.[250] The total heat-flow signal can then be deconvoluted to obtain one or more deconvoluted signals representative of, for example, the rapidly reversible (AC) and/or nonrapidly reversible (DC) components of the heat flow.[17,250]

The main idea of the deconvolution procedure was the importance of disentangling the sample response, which depends on temperature from the response, which depends on rate of temperature changes.[251] The basis of MTDSC is according to simultaneously measuring the C_p of the sample using the response to the linear ramp and the response to the modulation and comparing those.[17,251] For the inert sample, there are no significant temperature gradients between the sample temperature sensor and the center of the sample; both methods should give the same value. The fact that during transitions, these two techniques give different values is interesting.[17]

The best-known advantages of MTDSC are the ability to separately measure one or more components of the total heat-flow signal; an improved ability, compared with conventional DSC, to measure transformations or other thermal events that are overlapped in temperature and/or in time; and improved resolution by allowing for the use of a relatively slow, underlying heating rate.[251] The most commonly encountered types of processes that are studied by MTDSC are in polymeric materials.[251] The appropriate specific kinetic functions could be obtained as chemical reactions and related processes, glass transitions, and polymer melting.[251]

The results of averaging the MHF signal are equivalent to conventional DSC and can be recovered.[251] The fact is important, as the information DSC provides is very useful. The sample's vibrational C_p, independently of any other process that is occurring, such as a chemical reaction, could be measured by looking at the in-phase response to the modulation.[17,251] This signal leads to C_p directly. Also, the out-of-phase response can be expressed as the kinetic or in complex notation, the imaginary C_p.[17] However, it is generally approximated by taking the derivative with respect to temperature of the heat flow generated by the reaction or other process.[251] This signal can be used to determine the activation energy for a reaction. The nonreversing signal gives a measure of the energy that arises from the chemical reaction.[17]

The T_g, as measured by the reversing C_p, is a function of frequency.[17] The T_t, as measured by the total C_p on cooling, is a function of cooling rate.[17] There is equivalence between these two observations, as changing the frequency of the modulation and the cooling rate alters the time-scale over which the measurement is made.[17] Aging below the glass transition produces an enthalpy loss that is recovered as a peak overlaid on the glass transition.[17] However, this aging does not, at low degrees of annealing, have a great effect on the reversing signal, and this is intuitively satisfactory, as the aging effect is not reversible on the time-scale of the modulation.[17,251]

Polymer melting is the result of a distribution of species, all melting at their equilibrium melting temperature, and subsequently, the enthalpy of melting is found in whole or, in part, in the reversing signal.[17] Principally, this type of melting behaves in a similar manner to C_p, where there is no cooling during the modulation cycle.[17] Hence, the reversing signal no longer has the same meaning as it does when considering chemical reactions and glass transitions, as the reversing signal contains a contribution from an essentially nonreversing process.[17]

GFMDSC

GFMDSC modulates a DSC by setting the properties of a gas in thermal contact with the sample and the reference in the calorimeter.[250] The device allows the use of MDSC at high modulation rates compared with the modulation rates used with MTDSC.[17]

The major heat-flow path between the sample or reference and the furnace is the purge gas in the furnace chamber.[250,252] The composition of the purge gas in the furnace chamber of a DSC cell is modulated by alternately purging the DSC with a high thermal conductivity gas (such as helium) and with a low thermal conductivity gas (such as nitrogen).[252,253] This characteristic modulates the properties of the calorimeter cell. When there is no heat flow between the sample or reference and the furnace,

because of equilibrium between the sample and reference with the furnace, the composition of the purge gas is irrelevant, and there is no modulated signal.[250,252,253] However, if the sample is not in thermal equilibrium with its surroundings, modulating the thermal conductivity of the purge gas modulates the flow of heat to the sample or reference and thus, produces a modulated signal.[252–254]

As typical DSC cells have relatively small volumes, MDSCs can be modulated at relatively high rates using this technique.[252–254] If the temperature of the furnace is modulated at one frequency, and the composition of the purge gas is modulated at substantially different frequency, then a multiplexed signal would be created.[250]

Instead of the flow rate, the temperature of the temperature-controlling gas is modulated.[250,252–255] A combination of furnaces may be used to obtain the desired sample and reference temperatures. For instance, a relatively large thermal mass furnace may be used for the linear portion of the sample and reference temperatures, and separate low thermal mass furnaces may be used to modulate the sample or reference temperatures. [250,252–255] As the thermal mass of the modulation furnaces is relatively low, the sample or reference temperatures can be modulated at relatively high modulation rates.[250]

The technique provides improved methods and apparatus for modulating the temperature of a sample or a reference in a MDSC.[250,252] Also, it is another characteristic of the device to modulate the heat flow to and from a sample and a reference in a MDSC by modulating the composition of the purge gas in the modulated calorimeter.[250,252] Additionally, the technique modulates the temperature of a sample or a reference in a MDSC by modulating the flow rate of a gas controlling the temperature of the sample or a reference in the modulated calorimeter.[250]

There are several ways for purge gas to contribute the experiments. For instance, the flowing gas helps to remove moisture or oxygen, which may accumulate and damage the cell over the time.[256] Also, the gas supplies for a smooth thermal blanket, which limits localized hot-spots that can lead to artifactual heat flow.[256] The purge gas exists for more efficient heat transfer between the constantan disc and the sample pan, resulting in more sensitivity and faster response time. Additionally, it helps to cool the cell so that faster cooling rates and wider modulation parameters may be obtained.[256]

In summary, this equipment could be used in MDSC or DSC mode to contribute the experiment in several ways, such as to help to remove moisture or oxygen that may accumulate and damage the cell over time, to provide a smooth thermal blanket that eliminates localized hot-spots, which can lead to artifactual heat flow, and to provide more efficient heat transfer between the constantan disc and the sample pan, resulting in more sensitivity and faster response time. In fact, the purge gas by this system helps to cool the cell so that faster cooling rates and wider modulation parameters may be achieved. Hence, to optimize the MDSC experiment and generate accurate and reproducible results, a flowing inert purge gas using this equipment should generally be applied.[255,256]

PNDSC

Traditional DSC requires relatively large amounts of test material, and thermal analyses on nanoscale samples are difficult; however, it is not impossible. Its application in nanoscience, where sample sizes are small, is rather limited.[11] As the properties of nanomaterials may differ significantly from their bulk counterparts, a DSC that is sensitive enough to probe nanoscale quantities is desirable.[9] On the other hand, traditional DSCs are limited to taking one measurement at a time, and a new sample must be loaded between each measurement. This severely limits the use of a traditional DSC in combinatorial studies at the nanoscale.[257]

PNDSC is a power-compensation DSC, which included a plurality of cell structures being used to define a selective region for calorimetric measurements of a nanomaterial.[19] Heating units have been positioned on the cell structures to provide the required energy to perform calorimetric analyses in each of the cell structures.[19] The cell structures and the heating units are arranged so as to allow the calorimetric system to perform, in a combinatorial manner, calorimetric measurements associated with the nanostructure.[258]

The calorimetric system is used for the combinatorial analysis of complex nanoscale material systems.[19] The PNDSC is a micro-machined array of calorimetric cells. This new approach to combinatorial calorimetry greatly expedites the analysis of nanomaterial thermal characteristics.[19] Additionally, a set of samples can be analyzed simultaneously, greatly reducing the time for such a study when compared with a conventional, one-at-a-time approach.[258]

PNDSC combines DSC and combinatorial analysis in a novel way, which is ideal for analyzing complex material systems.[19,258] The core of the system is micro-machined, which included a 5×5 array of calorimetric cells.[19,258] The system reduces the measurement time of complex nanomaterials by at least an order of magnitude.[19, 258] The device promises to revolutionize the development of such materials, providing the raw material data for nanoscience innovation and design.[19,258]

The calorimeter includes a heating element in a double-spiral pattern.[19] Such a layout will improve the thermal efficiency of the device and expand its capability for kinetic analyses.[19] Incorporation of vanadium oxide, which has a thermal coefficient of resistivity of $\sim$2%/K, will increase temperature measurement sensitivity, particularly in the range

compatible with biomaterials.[19] Additionally, microfluidic channels in this device expand its applicability to fluid samples.[258]

PPC

Two popular types of calorimeters are DSCs and isothermal titration calorimeters (ITCs).[11] DSC increases or decreases the temperature of the system at a given rate automatically, while monitoring any temperature differential that arises between the two cells.[11] Minute differences between the amount of heat absorbed or released by the sample cell in comparison with the reference cell can be measured and related to the test material.[11]

In ITC, the calorimeter maintains a constant temperature, and the concentration of an additional material added to the cells is changed.[6] The added substance could be a ligand, which is bonded to the test material in the sample cell.[6] The calorimeter measures the heat absorbed or released, as the newly introduced ligand binds to the test. Various information about the interaction between the test sample and the ligand (such as stoichiometry, binding constant, and heat of binding) can be determined by repeating the titration experiment using multiple additions of the ligand until binding is completed.[6]

The idea of PPC was formed in response to the following problems. First, the analysis of volumetric characteristics of biopolymers in dilute solution has always been difficult and needed tedious experiments using densitometric or dilatometric techniques to determine partial molar volumes. The latter, measuring volume changes for biopolymer unfolding, is also problematic and most often done using large, reinforced optical cells up to high pressures.[20] On the other hand, as the basic calorimeters can only collect data in response to changes in one intensive variable (i.e., temperature or concentration), the information that existing calorimeters obtain on the test sample is limited.[259]

The PPC calorimeter includes: a reference cell and a sample cell, where the reference cell contains a liquid, and the sample cell contains a solution that includes the liquid and a test substance[20]; varying the pressure above the liquid in the sample cell and the solution in the reference cell[20]; and determining a differential heat effect between the sample cell and the reference cell in response to a change in the pressure used by the pressure system.[20]

PPC measures heat change, resulting from a pressure change above a solution containing a dissolved substance.[20] It leads to considerably greater accuracy for measuring critical volumetric parameters of, e.g., biopolymers in solution.[20] Also, it provides information about biopolymer solvation currently unavailable from any other techniques.[20] Additionally, PPC calorimeter obtains data resulting from variations in either of two intensive variables: temperature and pressure.[20]

The device uses small pressure perturbation to solutions in a reference cell and a sample cell at different temperatures and compares the heat absorbed or released by the two cells in response to each pressure perturbation .[20] Certain thermodynamic properties of the test substance in the sample cell can be assessed through these measurements. For instance, some PPC methods are particularly useful for determining the thermal coefficient of expansion of a macromolecule[260] and for determining the macromolecule's volume change as it unfolds.[20] The thermal coefficient of expansion of the substance at the known temperature could be obtained using the first and second laws of thermodynamics.[20] However, these terms cannot be measured with sufficient accuracy using existing technology.[259]

Technically, PPC includes a sample cell, a reference cell, and a pressure system that applies a variable pressure to the sample cell.[20] Additionally, there is a pressure controller that controls the pressure applied by the pressure system to the sample cell.[20] The calorimeter includes a heat-monitoring system, which subsequently determines the differences between the amount of heat absorbed or released by the sample cell and by the reference cell.[20] This monitoring system has a temperature sensor that monitors a temperature differential between the cells when it arises in response to a change in the pressure used by the pressure system.[20]

The sample cell is a vessel shaped to contain a liquid and a test substance (e.g., a biopolymer), and the pressure system applies the variable pressure to a liquid-holding portion of it.[20] The reference cell is substantially identical in mass and volume to the sample cell, and it contains a liquid too.[20]

The calorimeter has an electrical controller that is electrically coupled to the pressure controller.[20] The electrical control system includes a software program, which causes the pressure controller to periodically vary the pressure used by the pressure system.[20] Also, the computer program keeps in memory information sufficient to calculate the temperature differentials between the sample and reference cells.[20]

Unfolding studies of proteins and protein stability analysis is one of the most prominent applications of PPC.[259–262] As a protein unfolds by heating to a temperature higher than its melting point, the volume of the molecule changes, as hydrophobic side-chains ordinarily buried within the native protein are exposed to the exterior, and becomes solvated.[261] This volume change is an important structural parameter and is measurable using PPC. As Palma and Curmi[262] have indicated, the thermal expansion between folding and unfolding of proteins can help to

explain and predict protein stability. Hence, the thermal expansion from the heat released or absorbed after short pressure pulses on protein solutions would be obtainable.[263] Therefore, the data are useful in some applications, such as bioengineering studies.[260,261]

PPC can also be used to determine the coefficient of thermal expansion and the volume change for molecules other than proteins.[258] The volume change can be measured for molecules that undergo a structural transition driven by temperature, such as DNA and RNA,[264] or certain lipid vesicles,[265] carbohydrates,[266] or synthetic polymers.[267] Thermal coefficients are calculated for essentially any organic or inorganic substance, including any solute in an aqueous or nonaqueous solvent.[258,262]

SRDSC

The idea of SRDSC was formed because of one disadvantage of the power-compensation systems. The problem was their effectiveness over the temperature range–170 to 730°C. Hence, the development of higher temperature DSC calorimeters has concentrated on the heat-flux design,[11] and the self-referencing DSC was an embodiment to solve this weakness.

SRDSC technique, as a heat-flux DSC, was applied, in which the difference in heat-flow rate between the sample and the furnace is monitored against time or temperature, and the sample is subjected to a temperature program.[11] Self-referencing DSC is a high-quality, medium-range temperature, low-cost DSC, which is used in industrial characterization and materials study.[21] The heat-flux calorimeter measures the heat flow across a circular plate within a circular furnace in the uniform set.[21] The heat is transferred between the furnace and the sample through the flat plate, which has a central sample location whose temperature is monitored by a thermocouple.[21]

Multiple radial thermocouples are provided, centrally located under the sample cell, and at four reference parts at a certain distance between the furnace walls and the middle of the plate.[11] The thermocouples provide an averaged temperature signal from which the differential signal may be derived. The signal is directly proportional to the heating rate and the C_p of the sample.[11] Additionally, it should show improved baseline reproducibility, as there is less systematical thermal asymmetry.[11]

SRDSC has a single position in its center to place a sample, but it has no place for a reference.[11] This absence avoids any baseline inconsistency as a result of device asymmetry, and also, it nullifies any thermal noise at interface of the reference plate.[11]

For demonstrating the ability of the SRDSC, the physical aging of amorphous polyethylene terephthalate (PET) was carried out at 338 K to measure low-energy transition compared wiht power-compensation DSC.[21] The temperature at specific times would be raised at 10 K min^{-1}, through the glass transition, to 368 K and back to 338 K at 2.5 K min^{-1}. The process was repeated immediately to obtain the unaged glass transition, which was subtracted from each physical aging peak, and the remaining area was associated with the enthalpy of physical aging. SRDSC curves of PET at various stages of physical aging caused by physical aging were clearly significant, and the results were the same as those for power-compensation DSC reported previously.[268]

HPer DSC

As the conventional DSC has weakness in achieving highly controlled, constant rates in cooling, the idea of supplying a DSC that can operate a bit faster or even at much higher heating rates has received a great deal of attention.[22] The most important reasons for this aim include: most processes occur at much higher rates than are usable by conventional DSC, and some polymers and pharmaceuticals are in metastable states.[22] Hence, the idea of HPer DSC was formed to realize suitable conditions and correlate the results of thermal analyses to make improvements in the product characteristics.[269] In other words, HPer DSC (hyper DSC/high-speed DSC) can clarify metastability phenomena and solve its related problems.[269,270]

Instrumentally, the increasing rates need a decreasing size of related components of the measuring device (such as measuring cell) to extend the thermal conductivity paths.[22,271] In addition, decreasing the sample mass up to 1 μg is the other essential requirement. Consequently, this type of calorimeter should have a small furnace and offers the advantage of the power compensation in design.[22] Thus, it provides direct flow-rate assessments and the ideal temperature control on the sample for significant results.[271]

The existing HPer DSC, so-named power compensation Pyris 1 or Diamond DSC, has small furnaces and then precisely regulated cooling and heating rates, based on that fact that the temperature range of the measurements and the accessories have been used for cooling, respectively.[22,271] Also, developing the high-speed pulse-calorimeter has realized the extremely high heating rates up to 6×10°C/min.[22] In addition, development of the ultra-fast chip DSC led to the use of subnanograms of materials to achieve constant heating and cooling rates.[22]

Obtaining realistic conditions is a major challenge that occurs, for example, in high cooling rates in polymer processing.[22,272] Various phenomena influence verification and crystallization of the polymer. Hence, measuring under realistic conditions by HPer DSC realizes the use of high heating rates and mimics practical conditions.[22,273]

Another challenge that can be met by HPer DSC is metasta-

bility of macromolecules and pharmaceuticals.[20,274] Metastability correlates to common phenomena known in thermal analyses of the materials, such as hot or cold crystallizations, recrystallization, supercoiling, amorphization, and annealing.[22,274] Understanding the kinetics of metastability, related processes can be realized using the HPer DSC technique.[22,274] For instance, Vanden Poel and Mathot[270] have shown that the technique could be used as a powerful analytical tool for the study of this phenomenon in polymer studies. They investigated the crystallization and melting behavior of some well-known polymers (such as polypropylene, polyoxymethylene, and polyamide 6 in nano- or micrometer scales) using HPer DSC with consideration of a variety of cooling and heating rates.[269] The study cleared the capability of using accurate conditions of low or high and cooling or heating rates to assess the metastability of polymers and their related kinetics of transitions in detail.[269]

Many advantages by HPer DSC have been reported in literature.[22] The best known of these benefits include increased sensitivity,[22,271] increased production,[22,272,273] quantitative measurements of C_p and crystallinity,[22,275] studying of kinetics,[22,272] studying of reorganization phenomena,[22,273] preventing of undesired cold crystallization and recrystallization,[22,276] solid-solid transformations,[22,269,272,277] matching rates occurring routinely,[22,278] mimicking of rates in processing, such as extrusion and injection molding,[22,269,276,277] and measuring minute amounts of materials (e.g., amorphous content in predominantly crystalline samples) less than a few micrograms in practice.[22,271,279,280]

CONCLUSIONS

DSC is a powerful technique for obtaining the thermoanalytical parameters of biomolecules and nanomaterials.[74,76,138,211,224] Additionally, recent advances have made it possible to assess the purification yield of some pharmaceutical drugs such as antibodies.[122,124]

As the best-known goal of systems biology is to investigate new, emergent characteristics that may arise from the systemic view of a biological system,[281] DSC techniques could be useful to provide new data about the structural thermodynamics of reaction intermediates. In particular, some reactions, such as isothermal amplification of nucleic acids, may be processed in DSC and used to obtain new, thermodynamic information about nucleic acids while the molecules are polymerizing.[282]

As a thermoanalytical method, the technology can predict stability of biomolecules in various environmental conditions such as pH, ionic strength, and osmolites.[2,73,128,283–285] Some types of this instrument can reveal volumetric features of the sample in different pressures.[11] In addition, the interaction of biomolecules and nanoparticles could be tracked via the calorimeters.

Various types of calorimeters have been developed, and their applications could improve the thermoanalysis of a wide range of materials. On the other hand, in the last decades, considerable progress has been made in applications of DSCs in microfluidics, drug discovery, pharmaceuticals, molecular biology, and nanoscience.[11]

In conclusion, the combination of calorimetric techniques available to measure the thermodynamics of folding and unfolding transitions includes thermal scanning (DSC), pressure scanning (PPC), and isothermal (ITC) methods.[75,266] These instruments measure thermodynamic parameters, largely depending on different temperature and pressure ranges. Hence, the measurements may correspond to different sets of thermodynamic end states, thus complicating comparison of measured parameters from different samples.

ACKNOWLEDGMENT

The present study was partly supported by Tarbiat Modares University and Iranian Nanotechnology Initiative Council (INIC). We are also grateful to Amir-Hossein Taghavi for discussing the manuscript.

REFERENCES

1. Hohne G, Hemminger W, Flammersheim H-J. *Differential Scanning Calimetry: An Introduction for Practitioners*. Berlin, Germany: Springer-Verlag, 1996.
2. Privalov PL, Potekhin SA. Scanning microcalorimetry in studying temperature-induced changes in proteins. *Methods Enzymol* 1986;131:4–51.
3. Even J, Bertault M, Girard A, Délugeard Y, Marqueton Y. Optical and calorimetric studies on the role of lattice mode softening in assisting a thermally enhanced solid state reaction. *Chem Phys Lett* 1997;267:585–589.
4. Lin LN, Mason AB, Woodworth RC, Brandts JF. Calorimetric studies of the N-terminal half-molecule of transferrin and mutant forms modified near the Fe(3+)-binding site. *Biochem J* 1993;293:517–522.
5. Protasevich I, Ranjbar B, Lobachov V, et al. Conformation and thermal denaturation of apocalmodulin: role of electrostatic mutations. *Biochemistry* 1997;36:2017–2024.
6. Ladbury JE Chowdhry BZ. Sensing the heat: the application of isothermal titration calorimetry to thermodynamic studies of biomolecular interactions. *Chem Biol* 1996;3:791–801.
7. Von Stockar U, Marison IW. The use of calorimetry in biotechnology. *Bioprocess Eng* 1989;40:93–136.
8. Weber PC, Salemme R. Applications of calorimetric methods to drug discovery and the study of protein interactions. *Curr Opin Struc Biol* 2003;13:115–121.
9. Varghesea N, Vivekchanda SRC, Govindaraja A, Rao CNR. A calorimetric investigation of the assembly of gold nanorods to form necklaces. *Chem Phys Lett* 2008;450:340–344.
10. Haynie DT. *Biological Thermodynamics.* Cambridge, UK: Cambridge University Press, 2008.
11. Haines PJ, Reading, M, Wilburn FW. Differential thermal analysis and differential scanning calorimetry. In Brown ME (ed): *Handbook of Thermal Analysis and Calorimetry*, vol 1. The Netherlands: Elsevier Science BV, 1998;279–361.
12. Danley RL. New heat flux DSC measurement technique. *Thermochim Acta* 2002;395:201–208.
13. Zucca N, Erriu G, Onnis S, Longoni A. An analytical expression of the output of a power-compensated DSC in a wide temperature range. *Thermochim Acta* 2002;143:117–125.

14. Danley RL. *Differential Scanning Calorimeter*, European Patent 1 139 083 A1, 2001.
15. Wang L, Zhao Y, Ng E, Lid Q. A MEMS differential calorimeter for biomolecular characterization. *Proceedings of the IEEE International Conference on Micro Electro Mechanical Systems (MEMS*), Art. No. WP39, 2005;814–817.
16. Danley RL. *Infrared Heated Differential Scanning Calorimeter*, World Patent 2008 153 910 (A1), 2008.
17. Reading M, Hourston DJ. *Modulated-Temperature Differential Scanning Calorimetry.* New York, NY, USA: Springer, 2006.
18. Reading M. *Method and Apparatus for Gas Flow Modulated Differential Scanning Calorimetry*, US Patent 0 056 241 87 A, 1997.
19. Vlassak JJ, McCluskey PJ. *Parallel Nano-Differential Scanning Calorimetry*, US Patent 2007 286 769 A1, 2007.
20. Plotnikov VV, Brandts JF, Brandts JM. *Pressure Perturbation Calorimetry Instruments and Methods*, US Patent 2004 024 542 A1, 2004.
21. Holland BJ, Atkinson JR, Hay JN. Design and development in self-reference differential scanning calorimetry. *J Therm Anal Calorim* 2002;69:371–385.
22. Mathota VBF, Vanden Poel G, Pijpers TFJ. Benefits and potentials of high performance differential scanning calorimetry (HPer DSC). In Brown M, Gallagher P (eds): *Handbook of Thermal Analysis and Calorimetry*, vol 5. The Netherlands: Elsevier, 2007;269–297.
23. Horiuchi K. DSC studies on structural phase transitions and molecular motions in some A2MCl4 compounds. *Phys Status Solidi A* 2004;210:723–726.
24. Charsley EL, Laye PG, Palakollu V, Rooney JJ, Joseph B. DSC studies on organic melting point temperature standards. *Thermochim Acta* 2006;446:29–32.
25. Illers K-H Kanig G. Heat of fusion and lamellar structure of polyethylene single crystal mats. *Colloid Polym Sci* 1982;260: 564–569.
26. Adem E, Rickards J, Burillo G, Avalos-Borja M. Changes in poly-vinylidene fluoride produced by electron irradiation. *Radiat Phys Chem* 1999;54:637–641.
27. Vaikousi H, Lazaridou A, Biliraderis CG, Zawistowski J. Phase transitions, solubility, and crystallization kinetics of phytosterols and phytosterol-oil blends. *J Agric Food Chem* 2007;55:1790–1798.
28. Pérez-Alonso C, Cruz-Olivares J, Barrera-Pichardo JF, Rodríguez-Huezo ME, Báez-González JG, Vernon-Carter EJ. DSC thermo-oxidative stability of red chili oleoresin microencapsulated in blended biopolymers matrices. *J Food Eng* 2008; 85:613–624.
29. Privalov PL. Microcalorimetry of proteins and their complexes. In Shriver JW (ed): *Protein Structure, Stability, and Interactions*, vol 490. Totowa, NJ, USA: Humana Press, 2009;1–40.
30. Yakovlev GI, Moiseyev GP, Protasevich II, et al. Dissociation constants and thermal stability of complexes of *Bacillus intermedius* RNase and the protein inhibitor of *Bacillus amyloliquifaciens* RNase. *FEBS Lett* 1995;366:156–158.
31. Pfeil W. *Protein Stability and Folding: A Collection of Thermodynamic Data*. Berlin Heidelberg, Germany: Springer-Verlag, 1998.
32. He Y. DSC and DEA studies of under fill curing kinetics. *Thermochim Acta* 2001;367–368:101–106.
33. Van Holde KE, Curtis Johnson W, Shing Ho P. Thermodynamics and biochemistry. In *Principles of Physical Biochemistry*, 2nd ed. Upper Saddle River, NJ, USA: Pearson Prentice Hall, 2006;72–105.
34. Cooper A, Nutley MA, Walood A. Differential scanning microcalorimetry. In Harding SE, Chowdhry BZ (eds): *Protein-Ligand Interactions: Hydrodynamics and Calorimetry*. Oxford, UK: Oxford University Press, 2000;287–318.
35. Cooper A. *Biophysical Chemistry*. London, UK: Royal Society of Chemistry, 2004;103–107.
36. Cooper A. Heat capacity of hydrogen-bonded networks: an alternative view of protein folding thermodynamics. *Biophys Chem* 2000;85:25–39.
37. Cooper A, Johnson CM, Lakey JH, Nollmann M. Heat does not come in deferent colors: entropy-enthalpy compensation, free energy windows, quantum confinement, pressure perturbation calorimetry, salvation and the multiple causes of heat capacity effects in biomolecular interactions. *Biophys Chem* 2001;93: 215–230.
38. Cooper A. Microcalorimetry of protein-DNA interactions. In Travers A, Buckle M (eds): *DNA-Protein Interactions*. Oxford, UK: Oxford University Press, 2000;125–139.
39. Ford JL, Willson BR. Thermal analysis and calorimetry of pharmaceuticals. In Kemp R (ed): *Handbook of Thermal Analysis and Calorimetry,* vol 4. The Netherlands: Elsevier, 1999;923–1016.
40. Sturtevant J. Biochemical applications of differential scanning calorimetry. *Annu Rev Phys Chem* 1987;38:463–488.
41. Haynie DT, Freire E. Estimation of the folding/unfolding energetics of marginally stable proteins using differential scanning calorimetry. *Anal Biochem* 1994b;216:33–41.
42. Pilch DS. Calorimetry of nucleic acids. In Egli M, Herdewijn P, Matsuda A, et al. (eds): *Current Protocols in Nucleic Acid Chemistry*. New York, NY, USA: John Wiley & Sons, 2000;7.4.1–7.4.9.
43. Edsall TJ, Gutfreund H. Calorimetry, heat capacity, and phase transitions. In Edsall TJ, Gutfreund H (eds): *Biothermodynamics: The Study of Biochemical Processes at Equilibrium*. New York, NY, USA: John Wiley & Sons, 1983;210–227.
44. Breslauer KJ, Freier E, Straume M. Calorimetry: a tool for DNA and ligand-DNA studies. *Methods Enzymol* 1992;211:533–567.
45. Krug RR, Hunter WG, Grieger RA. Enthalpy-enthropy compensation. 1. Some fundamental statistical problems associated with the analysis of van't Hoff and Arrhenius data. *J Phys Chem* 1976;80:2335–2341.
46. Kholodenko V. A simple method to measure the absolute heat capacity of proteins. *Anal Biochem* 1999;270:336–338.
47. Shortle D, Ackerman MS. Persistence of native-like topology in a denatured protein in 8 M urea. *Science* 2001;293:487–489.
48. Baldwin RL. Protein folding: making a network of hydrophobic clusters. *Science* 2002;295:1657–1658.
49. Klein-Seetharaman J, Oikawa M, Grimshaw SB, et al. Interactions within a nonnative protein. *Science* 2002;295:1719–1722.
50. Privalov PL, Dragan AI. Microcalorimetry of biological macromolecules. *Biophys Chem* 2007;126:16–24.
51. Cueto M, Dorta MJ, Munguía O, Llabrés M. New approach to stability assessment of protein solution formulations by differential scanning calorimetry. *Int J Pharm* 2003;252:159–166.
52. Sánchez-Ruíz JM, López-Lacomba JL, Cortijo M, Mateo PL. Differential scanning calorimetry of the irreversible thermal denaturation of thermolysin. *Biochemistry* 1988;27:1648–1652.
53. Conejero-Lara F, Sánchez-Ruíz JM. Differential scanning calorimetry study of carboxypeptidase B, procarboxypeptidase B and its globular activation domain. *Eur J Biochem* 1991;200:663–670.
54. Cooper A, McAuley KE. Microcalorimetry and the molecular recognition of peptides and proteins. *Phil Trans R Soc Lond A* 1993;345:23–35.
55. Sanz JM, García JL, Laynez J, Usobiaga P, Menéndez M. Thermal stability and cooperative domains of CPL 1 lysozyme and its NH2- and COOH-terminal modules. *J Biol Chem* 1993;268: 6125–6130.
56. Martínez JC, Filimonov VV, Mateo PL, Schreiber G, Fersht AL. A calorimetric study of the thermal stability of Barstar and its interaction with Barsane. *Biochemistry* 1995;34:5224–5233.

57. Tello-Solìs SR, Hernández-Arana A. Effects of irreversibility on the thermodynamic characterization of the thermal denaturation of *Aspergillus saitoi* acid proteinase. *J Biochem* 1995;311: 969–974.
58. Conejero-Lara F, Mateo PL. Presence of a low dimerization equilibrium on the thermal unfolding of the 205–316 thermolysin fragment at neutral pH. *Biochemistry* 1996;35:3477–3486.
59. Funahashi J, Takamo K, Ogosahara K, Yamagata Y, Yutani K. The structure, stability and folding process of amyloidogenic mutant human lysozyme. *J Biochem* 1996;120:1216–1223.
60. Libouga DG, Aguie-Beghin V, Douillard R. Thermal denaturation and gelation of rubisco: effects of pH and ions. *Int J Biol Macromol* 1996;19:271–277.
61. Kulmyrzaev A, Bryant C, McClements DJ. Influence of sucrose on the thermal denaturation, gelation, and emulsion stabilization of whey proteins. *J Agric Food Chem* 2000;48:1593–1597.
62. Takano K, Yamagata Y, Kubota M, Funahashi J, Fujii S, Yutani K. Contribution of hydrogen bonds to the conformational stability of human lysozyme: calorimetry and X-ray analysis of six Ser → Ala mutants. *Biochemistry* 1999;38:6623–6629.
63. Takano K, Yamagata Y, Fujii S, Yutani K. Contribution of the hydrophobic effect to the stability of human lysozyme: calorimetric studies and X-ray structural analyses of the nine valine alanine mutants. *Biochemistry* 1997;36:688–698.
64. Vogl T, Jatzke C, Hinz HJ, Benz J, Huber R. Thermodynamic stability of annexin VE17G: equilibrium parameters from an irreversible unfolding reaction. *Biochemistry* 1997;36:1657–1668.
65. Remmele RL, Gombotz WR. Differential scanning calorimetry: a practical tool for elucidating the stability of liquid biopharmaceuticals. *Pharm Tech Eur* 2000;12:56–65.
66. Cooper A. Effect of cyclodextrins on the thermal stability of globular proteins. *J Am Chem Soc* 1992;114:9208–9209.
67. Sánchez-Ruíz JM. Theoretical analysis of Lumry–Eyring models in differential scanning calorimetry. *Biophys J* 1992;61:921–935.
68. Azuaga AI, Sepulcre F, Padrós E, Mateo PL. Scanning calorimetry and Fourier-transform infrared studies into the thermal stability of cleaved bacteriorhodopsin systems. *Biochemistry* 1996;35:16328–16335.
69. Remmele RL, Nightlinger NS, Srinivasan S, Gombotz W. R. Interleukin-1 receptor (IL-1R) liquid formulation development using differential scanning calorimetry. *Pharm Res* 1998;15: 200–208.
70. Branchu S, Forbes RT, York P, Nyqvist H. A central composite design to investigate the thermal stabilization of lysozyme. *Pharm Res* 1999;16:702–708.
71. Griko YV, Makhatadze GI, Privalov PL, Hartley RW. Thermodynamics of barnase unfolding. *Protein Sci* 1994;3:669–676.
72. Wintrode PL, Makhatadze GI, Privalov PL. Thermodynamics of ubiquitin unfolding. *Proteins* 1994;18:246–253.
73. Schulga A, Kurbanov F, Kirpichinikov M, et al. Comparative study of binase and barnase: experience in Chimeric ribonucleases. *Protein Eng* 1998;11:775–782.
74. Ranjbar B, Protasevich II, Shulga AA, et al. Barnase, binase, and their hybrids: differences in conformation and heat denaturation parameters. *Mol Biol (Moscow)* 1997;31:413–419.
75. Afshar M, Caves L, Guimard L, et al. Investigating the high affinity and low sequence specificity of calmodulin binding to its targets. *J Mol Biol* 1994;244:554–571.
76. Mikulecky PJ, Feig AL. Heat capacity changes associated with nucleic acid folding. *Biopolymers* 2006;82:38–58.
77. Privalov PL, Plotnikov VV, Filimonov VV. Precision scanning microcalorimeter for the study of liquids. *J Chem Thermodyn* 1975;7:41–47.
78. Jelesarov I, Crane-Robinson C, Privalov PL. The energetics of HMG box interactions with DNA: thermodynamic description of the target DNA duplexes. *J Mol Biol* 1999;294:981–995.
79. Wu P, Sugimoto N. New thermodynamic characterization and transition mechanism of DNA duplex formation. *Nucleic Acids Res* 2000;44:15–16.
80. Filimonov VV, Privalov PL. Thermodynamics of base interaction in (A)n and (A.U)n. *J Mol Biol* 1978;122:465–470.
81. Ulkowski M, Musialik M, Litwinienko G. Use of differential scanning calorimetry to study lipid oxidation. 1. Oxidative stability of lecithin and linolenic acid. *J Agric Food Chem* 2005; 53:9073–9077.
82. Nelson DL, Cox MM. (eds): *Lehninger Principles of Biochemistry*. New York, NY, USA: Freeman, 2004.
83. Alberts B, Johnson A, Lewis J, Raff M, Roberts K, Walter P. (eds): *Molecular Biology of the Cell.* New York, NY, USA: Garland Science, 2002.
84. Smith EL, Hill RL, Lehman IR, Lefkowitz RJ, Handler P, White A. (eds): *Principles of Biochemistry*, 7th ed. New York, NY, USA: McGraw-Hill, 1983.
85. Dopico AM. (ed): *Methods in Membrane Lipids.* New York, NY, USA: Springer, 2007.
86. Heinz E. Plant glycolipids: structure, isolation and analysis. In Christie WW (ed): *Advances in Lipid Methodology*—3. Dundee, Scotland, Oily Press, 1996;211–332.
87. Hölzl G, Dörmann P. Structure and function of glycoglycerolipids in plants and bacteria. *Prog Lipid Res* 2007;46:225–243.
88. Brasaemle DL. Thematic review series: adipocyte biology. The perilipin family of structural lipid droplet proteins: stabilization of lipid droplets and control of lipolysis. *J Lipid Res* 2007;48: 2547–2559.
89. Wang X. Lipid signaling. *Curr Opin Plant Biol* 2004;7:329–336.
90. Eyster KM. The membrane and lipids as integral participants in signal transduction. *Adv Physiol Educ* 2007;31:5–16.
91. Hinkovska-Galcheva V, VanWay SM, Shanley TP, Kunkel RG. The role of sphingosine-1-phosphate and ceramide-1-phosphate in calcium homeostasis. *Curr Opin Invest Drugs* 2008;9:1192–1205.
92. Boyce JA. Eicosanoids in asthma, allergic inflammation, and host defense. *Curr Mol Med* 2008;8:335–349.
93. Beltowski J. Liver X receptors (LXR) as therapeutic targets in dyslipidemia. *Cardiovas Ther* 2008;26:297–316.
94. Saddoughi SA, Song P, Ogretmen B. Roles of bioactive sphingolipids in cancer biology and therapeutics. *Subcell Biochem* 2008;49:413–440.
95. Indiveri C, Tonazzi A, Palmieri F. Characterization of the unidirectional transport of carnitine catalyzed by the reconstituted carnitine carrier from rat liver mitochondria. *Biochim Biophys Acta* 1991;1069:110–116.
96. Parodi AJ, Leloir LF. The role of lipid intermediates in the glycosylation of proteins in the eucaryotic cell. *Biochim Biophys Acta* 1979;559:1–37.
97. Helenius A, Aebi M. Intracellular functions of N-linked glycans. *Science* 2001;291:2364–2369.
98. Gohil VM, Greenberg ML. Mitochondrial membrane biogenesis: phospholipids and proteins go hand in hand. *J Cell Biol* 2009;184:469–472.
99. Hoch FL. Cardiolipins and biomembrane function. *Biochim Biophys Acta* 1992;1113:71–133.
100. Kowalski B. Thermoanalytical investigations of edible oils and fats. I. Kinetics of thermal-oxidative decomposition of rapeseed oil. *Acta Aliment Polon* 1988;14:195–206.
101. Kowalski B. Thermal-oxidative decomposition of edible oils and fats. DSC studies. *Thermochim Acta* 1991;184:49–57.
102. Kasprzycka-Guttman T, Odzeniak D. Thermoanalytical investigation of edible oil. *Thermochim Acta* 1992;204:303–310.
103. Kasprzycka-Guttman T, Odzeniak D. Isothermal DSC investigation of the kinetics of thermoxidative decomposition of some edible oils. *J Therm Anal* 1993;39:217–220.

104. Adhvaryu A, Erhan SZ, Liu ZS, Perez JM. Oxidation kinetic studies of oils derived from unmodified and genetically modified vegetables using pressurized differential scanning calorimetry and nuclear magnetic resonance. *Thermochim Acta* 2000;364: 87–97.
105. Abd Karim A, Norziah MH, Seow CC. Review: methods for the study of starch gelatinisation. *Food Chem* 2000;71:9–36.
106. Blanshard JMV. Starch granule structure and function: a physicochemical approach. In Galliard T (ed): *Starch Properties and Potentials. Critical Reports on Applied Chemistry*, vol 13. London, UK: Society of Chemical Industry, 1987;16–54.
107. Fukuoka M, Ohta K-I, Watanabe H. Determination of the terminal extent of starch gelatinization in a limited water system by DSC. *J Food Eng* 2002;53:39–42.
108. Lai LS, Kokini JL. Physicochemical changes and rheological properties of starch during extrusion (a review). *Biotechnol Progr* 1991;7:251–266.
109. Olkku J, Rha C. Gelatinization of starch and wheat flour starch—a review. *Food Chem* 1973;3:293–311.
110. Sopade PA, Halley PJ, Junming LL. Gelatinization of starch in mixtures of sugars. II. Application of differential scanning calorimetry. *Carbohyd Polym* 2004;58:311–321.
111. Alavi S. Starch research over the years. *Food Res Int* 2003;36: 307–308.
112. Karapantsios TD, Sakonidou EP, Raphaelides SN. Water dispersion kinetics during starch gelatinization. *Carbohyd Polym* 2002;49:479–490.
113. Jenkins PJ, Donald AM. Gelatinization of starch: a combined SAXS/WAXS/DSC and SANS study. *Carbohyd Res* 1998;308: 133–147.
114. Liu Q, Charlet G, Yelle S, Arul J. Phase transition in potato starch—water system. I. Starch gelatinization at high moisture level. *Food Res Int* 2002;35:397–407.
115. Stevens DJ, Elton GAH. Thermal properties of the starch—water system. Part I. Measurement of heat of gelatinization by differential scanning calorimetry. *Starch-Stärke* 1971;23:8–11.
116. Biliaderis CG, Maurice TJ, Vose JR. Starch gelatinization phenomena studied by differential scanning calorimetry. *J Food Sci* 1980;45:1669–1680.
117. Donovan JW. Phase transitions of starch–water system. *Bioploymers* 1979;18:263–275.
118. Lelievre J. Theory of gelatinization in a starch–water solutes system. *Polymer* 1976;17:854–858.
119. Wootton M, Bamanuarachichi A. Application of differential scanning calorimetry to starch gelatinization. I. Commercial native and modified starches. *Starch-Stärke* 1979a;31:201–204.
120. Wootton M, Bamanuarachichi A. Application of differential scanning calorimetry to starch gelatinization. II. Effect of heating rate and moisture level. *Starch-Stärke* 1979b;31:262–264.
121. Wootton M, Bamanuarachichi A. Application of differential scanning calorimetry to starch gelatinization. III. Effect of sucrose and sodium chloride. *Starch-Stärke* 1980;32:126–129.
122. Harn N, Allan C, Oliver C, Middaugh CR. Highly concentrated monoclonal antibody solutions: direct analysis of physical structure and thermal stability. *J Pharm Sci* 2007;96:532–546.
123. Lobo ED, Hansen RJ, Balthasar JP. Antibody pharmacokinetics and pharmacodynamics. *J Pharm Sci* 2004;93:2645–2668.
124. Ejima D, Tsumoto K, Fukada H, et al. Effects of acid exposure on the conformation, stability, and aggregation of monoclonal antibodies. *Protein Struct Funct Genet* 2007;66:954–962.
125. Vermeer AWP, Norde W. The thermal stability of immunoglobulin: unfolding and aggregation of a multi-domain protein. *Biophys J* 2000;78;394–404.
126. Vlasov AP, Kravchuk ZI, Martsev SP. Non-native conformational states of immunoglobulins: thermodynamic and functional studies of rabbit IgG. *Biochemistry (Moscow)* 1996;61: 155–171.
127. Martsev SP, Kravchuk ZI, Vlasov AP, Lyakhnovich GV. Thermodynamic and functional characterization of a stable IgG conformer obtained by renaturation from a partially structured low pH-induced state. *FEBS Lett* 1995;361:173–175.
128. Calmettes P, Cser L, Rajnavolgyi E. Temperature and pH dependence of immunoglobulin conformation. *Arch Biochem Biophys* 1991;291:277–283.
129. Buchner J, Renner MR, Lilie H, et al. Alternatively folded states of an immunoglobulin. *Biochemistry* 1991;30:6922–6929.
130. Thies MJW, Kammermeier R, Richter K, Buchner J. The alternatively folded state of the antibody C(H)3 domain. *J Mol Biol* 2001;309:1077–1085.
131. Welfle K, Misselwitz R, Hausdorf G, Hohne W, Welfle H. Conformation, pH-induced conformational changes, and the thermal unfolding of anti-p24 (HIV-1) monoclonal antibody CB4-1 and its Fab and Fc fragments. *Biochim Biophys Acta* 1999;11431:120–131.
132. Martsev SP, Kravchuk ZI, Vlasov AP. Large increase in thermal stability of the CH3 domain of rabbit IgG after acid treatment as evidenced by differential scanning calorimetry. *Immunol Lett* 1994;43:149–152.
133. Tischenko VM, Xavyalov VP, Medgyesi GA, Potekhi SA, Privalov PL. A thermodynamic study of cooperative structures in rabbit immunoglobulin G. *Eur J Biochem* 1982;126:517–521.
134. Protasevich II, Ranjbar B, Varlamova EY, Cherkasov IA, Lapuk VA. Comparative study of monoclonal immunoglobulin M and rheumatoid immunoglobulin M by differential scanning microcalorimetry. *Biochemistry (Moscow)* 1997;62:914–918.
135. Yu L. Amorphous pharmaceutical solids: preparation, characterization and stabilization. *Adv Drug Del Rev* 2001;48:27–42.
136. Angell CA. The old problems of glass and the glass transition, and the many new twists. *Proc Natl Acad Sci USA* 1995;92: 6675–6682.
137. Byrn S, Pfeiffer R, Ganey M, Hoiberg C, Poochikian G. Pharmaceutical solids: a strategic approach to regulatory considerations. *Pharm Res* 1995;12:945–954.
138. Shah B, Kakumanu V, Bansal AK. Analytical techniques for quantification of amorphous/crystalline phases in pharmaceutical solids. *J Pharm Sci* 2006;95:1641–1665.
139. Saleki-Gerhardt A, Ahlneck C, Zografi G. Assessment of disorder in crystalline solids. *Int J Pharm* 1994;101:237–247.
140. Guinot S, Leveiller F. The use of MTDSC to assess the amorphous phase content of a micronized drug substance. *Int J Pharm* 1999;192:63–75.
141. Takahashi H, Chen R, Okamoto H, Danjo K. Acetaminophen particle design using chitosan and a spray-drying technique. *Chem Pharm Bull* 2005;53:37–41.
142. Phillips EM. An approach to estimate the amorphous content of pharmaceutical powders using calorimetry with no calibration standards. *Int J Pharm* 1997;149:267–271.
143. Lefort R, Gusseme AD, Willart JF, Danede F, Descamps M. Solid state NMR and DSC methods for quantifying the amorphous content in solid dosage forms: an application to ball-milling of trehalose. *Int J Pharm* 2004;280:209–219.
144. Kakumanu V, Bansal AK. Enthalpy relaxation studies of celecoxib amorphous mixtures. *Pharm Res* 2002;19:1873–1878.
145. Mooter GVD, Wuyts M, Blaton N, et al. Physical stabilization of amorphous ketoconazole in solid dispersions with polyvinylpyrrolidone K25. *Eur J Pharm Sci* 2001;12:261–269.
146. Hatta I. Conditions required for heat capacity measurements using modulated-temperature calorimetry. *Int J Pharm* 1999; 129:33–37.
147. Yousefi A, Eemaeili F, Rahimian S, Atyabi F, Dinarvand R. Preparation and in vitro evaluation of a pegylated nano-liposomal formulation containing docetaxel. *Sci Pharm* 2009;77:453–464.

148. Zhang H, Tong S-Y, Zhang X-Z, Cheng S-X, Zhuo R-X, Li H. Novel solvent-free methods for fabrication of nano- and microsphere drug delivery systems from functional biodegradable polymers. *J Phys Chem C* 2007;111:12681–12685.
149. Yu D-G, Shen X-X, Branford-White C, White K, Zhu L-M, Bligh SWA. Oral fast-dissolving drug delivery membranes prepared from electrospun polyvinylpyrrolidone ultrafine fibers. *Nanotechnology* 2009;20:055104.
150. Lu B, Xiong SB, Yang H, Yin XB, Chao RB. Solid lipid nanoparticles of mitoxantrone for local injection against breast cancer and its lymph node metastases. *Eur J Pharm Sci* 2006;28:86–95.
151. Müller RH, Rühl D, Runge SA. Biodegradation of solid lipid nanoparticles as a function of lipase incubation time. *Int J Pharm* 1996c;144:115–121.
152. Müller RH, Maassen S, Weyhers H, Specht F, Lucks JS. Cytotoxicity of magnetite loaded polylactide, polylactide/glycolide particles and solid lipid nanoparticles (SLN). *Int J Pharm* 1996b; 138:85–94.
153. Cavalli R, Gasco MR, Chetoni P, Burgalassi S, Saettone MF. Solid lipid nanoparticles (SLN) as ocular delivery system for tobramycin. *Int J Pharm* 2002;238:241–245.
154. Yang SC, Lu LF, Cai Y, Zhu JB, Liang BW, Yang CZ. Body distribution in mice of intravenously injected camptothecin solid lipid nanoparticles and targeting effect on brain. *J Control Release* 1999;59:299–307.
155. Hu F-Q, Zhang Y, Du Y-Z, Yuan H. Nimodipine loaded lipid nanospheres prepared by solvent diffusion method in a drug saturated aqueous system. *Int J Pharm* 2008;348:146–152.
156. Müller RH, Mäader K, Gohla S. Solid lipid nanoparticle (SLN) for controlled drug delivery-review of the state of the art. *Eur J Pharm Biopharm* 2000;50:161–177.
157. Olbrich C, Bakowsky U, Lehr CM, Muller RH, Kneuer C. Cationic solid-lipid nanoparticles can efficiently bind and transfect plasmid DNA. *J Control Release* 2001;77:345–355.
158. Müller RH, Lucks JS. *Arzneistoffträger aus festen lipid teilchen, Feste lipid nanosphäaren (SLN)*, European Patent 0 605 497, 1996a.
159. Jenning V, Andreas FT, Gohla SH. Characterization of a novel solid lipid nanoparticle carrier system based on binary mixtures of liquid and solid lipids. *Int J Pharm* 2000;199:167–177.
160. Jenning V, Gohla SH. Encapsulation of retinoids in solid lipid nanoparticles (SLN). *J Microencapsul* 2001;18:149–158.
161. Souto EB, Wissing SA, Barbosa CM, Müller RH. Development of a controlled release formulation based on SLN and NLC for topical clotrimazole delivery. *Int J Pharm* 2004;278:71–77.
162. Pichot C. Reactive nanocolloids for nanotechnologies and microsystems. In Elaissari A (ed): *Colloidal Nanoparticles in Biotechnology*, Malden, MA, USA: Wiley InterScience Publication, 2008;1–30.
163. Daniel MC, Astruc D. Gold nanoparticles: assembly, supramolecular chemistry, quantum-size-related properties, and applications toward biology, catalysis, and nanotechnology. *Chem Rev* 2004;104:293–346.
164. Bocanegra-Diaza A, Mohallem NDS, Novakb AM, Sinisterra RD. Preparation of ferrofluid from cyclodextrin and magnetite. *J Magn Magn Mater* 2004;272–276:2395–2397.
165. Wu M-L, Chen DH, Huang T-C. Preparation of Pd/Pt bimetallic nanoparticles in water/AOT/isooctane microemulsions. *J Colloid Interf Sci* 2001;243:102–108.
166. Yu Y, Qiu H, Wu X, et al. Synthesis and characterization of silica nanotubes with radially oriented mesopores. *Adv Funct Mater* 2008;18:541–550.
167. Bruchez MP, Hotz CZ. *Quantum Dots Applications in Biology.* Totowa, NJ, USA: Humana Press, 2007.
168. Gill P, Alvandi A-H, Abdul-Tehrani H, Sadeghizadeh M. Colorimetric detection of *Helicobacter pylori* DNA using isothermal helicase-dependent amplification and gold nanoparticle probes. *Diagn Micr Infec Dis* 2008;62:119–124.
169. Gill P, Ghalami M, Ghaemi A, Mosavari N, Abdul-Tehrani H, Sadeghizadeh M. Nanodiagnostic method for colorimetric detection of *Mycobacterium tuberculosis* 16S rRNA. *Nanobiotechnol* 2008;4:28–35.
170. Tanimoto A. Magnetic resonance imaging with supermagnetic nanocapsules. In Arshady R (ed): *Microspheres Microcapsules & Liposomes*, vol 3. London, UK: Citus Books, 2001;525–556.
171. Fritzsche W, Taton TA. Metal nanoparticles as labels for heterogeneous, chip-based DNA detection. *Nanotechnology* 2003;14: 63–73.
172. Wang J-X, Wen L-X, Wang Z-H, Wang M, Shao L, Chen J-F. Facile synthesis of hollow silica nanotubes and their application as supports for immobilization of silver nanoparticles. *Scripta Mater* 2004;51:1035–1039.
173. Michalet X, Pinaud FF, Bentolila LA, et al. Peptide coated semiconductor nanocrystals for biomedical applications. *Proc SPIE* 2005;5704:57–68.
174. Liu Z, Tabakman S, Welsher K, Dai H. Carbon nanotubes in biology and medicine: in vitro and in vivo detection, imaging and drug delivery. *Nano Res* 2009;2:85–120.
175. Vögtle F, Richardt G, Werner N. *Dendrimer Chemistry.* Weinheim, Germany: Wiley-VCH Verlag GmbH & Co. KGaA, 2009.
176. Mincheva R, Manolova N, Paneva D, Rashkov I. Novel polyelectrolyte complexes between N-carboxyethylchitosan and synthetic polyelectrolytes. *Eur Polym J* 2005;42:858–868.
177. Kwon GS, Okano T. Soluble self-assembled block copolymers for drug delivery. *Pharm Res* 1999;16:597–600.
178. Mehnert W, Mäder K. Solid lipid nanoparticles: production, characterization and applications. *Adv Drug Deliv Rev* 2001;47: 165–196.
179. Cardoso AH, Paula Leite CA, Darbello Zaniquelli ME, Galembeck F. Easy polymer latex self-assembly and colloidal crystal formation: the case of poly[styrene-co-(2-hydroxyethyl methacrylate)]. *Colloid Surface A* 1998;144:207–217.
180. Singh R, Pantarotto D, McCarthy D, et al. Binding and condensation of plasmid DNA onto functionalized carbon nanotubes: toward the construction of nanotube-based gene delivery vectors. *J Am Chem Soc* 2005;127:4388–4396.
181. Hui H, Xiao-dong F, Zhong-lin C. Thermo- and pH-sensitive dendrimer derivatives with a shell of poly(N,N-dimethylaminoethyl methacrylate) and study of their controlled drug release behavior. *Polymer* 2005;46:9514–9522.
182. Buchhammer H-M, Mende M, Oelmann M. Formation of mono-sized polyelectrolyte complex dispersions: effects of polymer structure, concentration and mixing conditions. *Colloid Surface A* 2003;218:151–159.
183. Li XY, Kong XY, Shi S, et al. Preparation of alginate coated chitosan microparticles for vaccine delivery. *BMC Biotechnol* 2008;8:89.
184. Almeidaa AJ, Souto E. Solid lipid nanoparticles as a drug delivery system for peptides and proteins. *Adv Drug Deliver Rev* 2007;59:478–490.
185. Kissel T, Li Y, Unger F. ABA-triblock copolymers from biodegradable polyester A-blocks and hydrophilic poly (ethylene oxide) B-blocks as a candidate for in situ forming hydrogel. *Adv Drug Deliv Rev* 2002;54:99–134.
186. Satohc MS, Moriyamac C, Asaia A, et al. Monoclonal antibody-mediated solid-phase assay for mammalian O6-alkylguanine DNA alkyltransferase activity. *Anal Biochem* 1991;196:403–409.
187. Bao H, Chen Z, Liu J. Fabrication of nanoscale latex arrays based on hydroxylated poly(butyl methacrylate- b-glycidyl methacrylate). *Colloid Polym Sci* 2004;282:92–95.

188. Lu A-H, Salabas EL, Schüth F. Magnetic nanoparticles: synthesis, protection, functionalization, and application. *Angew Chem Int Ed* 2007;46:1222–1244.
189. Tao L, Huna X, Zhang ZJ. Synthesis and characterization of new fluorescent nanoparticles. *Chinese Chem Lett* 2008;19:479–482.
190. Rouxa C, Chai F, Ollivier N, et al. Ti-C_p functionalization by deposition of organic/inorganic silica nanoparticles. *BiomolEng* 2007;24:549–554.
191. Hanisch C, Kulkarni A, Zaporojtchenko V, Faupel F. Polymer-metal nanocomposites with 2-dimensional Au nanoparticle arrays for sensoric applications. *J Phys Conf Ser* 2008;100:052043.
192. Meza M. Application of magnetic particles in immunoassays. In Hafeli U, Schutt W, Teller J, Zborowski M (eds): *Scientific and Clinical Applications of Magnetic Carriers*. New York, NY, USA: Plenum Press, 1997;303–309.
193. Elaissari A. Magnetic latex particles in nanobiotechnologies for biomedical diagnostic applications: state of the art. *Macromol Symp* 2009;281:14–19.
194. Harma H. Particle technologies. *Technol Rev* 2002;126:1–30.
195. Drake TJ, Zhao XJ, Tan W. Bioconjugated silica nanoparticles for bioanalytical applications. In Niemeyer CM, Mirkin CA (eds): *Nanobiotechnology*. Weinheim, Germany: Wiley-VCH Verlag GmbH & Co. KGaA, 2004.
196. Wenguang L, Jiab QX, Wanga H-L. Facile synthesis of metal nanoparticles using conducting polymer colloids. *Polym Commun* 2006;47:23–26.
197. Heurtault B, Saulnier P, Pech B, Proust J-E, Benoit J-P. Physicochemical stability of colloidal lipid particles. *Biomaterials* 2003;24:4283–4300.
198. Ranjbar B, Gill P. Circular dichroism techniques: biomolecular and nanostructural analyses—a review. *Chem Biol Drug Des* 2009;74:101–120.
199. Siekmann B, Westesen K. Thermoanalysis of the recrystallization process of melt-homogenized glyceride nanoparticles. *Colloid Surface B* 1994;3:159–175.
200. Eldem T, Speiser P, Hincal A. Optimization of spray-dried and congealed lipid micropellets and characterization of their surface morphology by scanning electron microscopy. *Pharm Res* 1991;8:47–54.
201. Wunderlich B. The thermal properties of complex, nanophase-separated macromolecules as revealed by temperature-modulated calorimetry. *Thermoch Acta* 2003;403:1–13.
202. Wunderlich B. Calorimetry of nanophases of macromolecules. *Int J Thermophys* 2007;28:958–967.
203. Gaur U, Wunderlich B. Study of microphase separation in block copolymers of styrene and α-methylstyrene in the glass transition region using quantitative thermal analysis. *Macromolecules* 1980;13:1618–1625.
204. Forrest JA, Mattsson J. Reductions of the glass transition temperature in thin polymer films: probing the length scale of cooperative dynamics. *Phys Rev E Stat Phys Plasmas Fluids Relat Interdiscip Topics* 2000;61:R53–R56.
205. Wunderlich B. Thermodynamics and properties of nanophases. *Thermochim Acta* 2008;492:2–15.
206. Meincken M, Balk LJ, Sanderson RD. Improved sensitivity in the thermal investigation of polymeric nanophases by measuring the resonance frequency shift using an atomic force microscope. *Macromol Mater Eng* 2001;286:412–420.
207. Mozafari MR. *Nanocarrier Technologies: Frontiers of Nanotherapy*. The Netherlands: Springer, 2006.
208. Bailey SE, Olin TJ, Bricka RM, Adrian DD. A review of potentially low-cost sorbents for heavy metals. *Water Res* 299;33:2469–2479.
209. Filho NC, Winkler-Hechenleitner AA, Gomez-Pineda EA. Copper (II) adsorption onto sugar cane bagasse. *Int J Polym Mater* 1996;34:211–218.
210. Peternele WS, Winkler-Hechenleitner AA, Gomez-Pineda EA. Adsorption of Cd(II) and Pb(II) onto functionalized formic lignin from sugar cane bagasse. *Bioresource Technol* 1999;68:95–100.
211. Varma AJ, Deshpande SV, Kennedy JF. Metal complexation by chitosan and its derivatives: a review. *Carbohyd Polym* 2004;55:77–93.
212. Knorr D, Sinskey A. Biotechnology in food production and processing. *Science* 1985;229:1224–1229.
213. Yang TC, Zall RR. Absorption of metals by natural polymers generated from seafood processing wastes. *Ind Eng Chem Prod Res Dev* 1984;23:168–172.
214. Masri MS, Reuter FW, Fiedman M. Interaction of wool with metal cations. *J Appl Polym Sci* 1974;18:675–681.
215. Nieto JM, Peniche-Covas C. Characterization of chitosan by pyrolysis-mass spectrometry, thermal analysis and differential scanning calorimetry. *Thermochim Acta* 1991;176:63–68.
216. Qu X, Wirsen A, Albertsson AC. Effect of lactic/glycolic acid side chains on the thermal degradation kinetics of chitosan derivatives. *Polymer* 2000;41:4841–4847.
217. Sreenivasan K. Thermal stability studies of some chitosan-metal ion complexes using differential scanning calorimetry. *Polym Degrad Stabil* 1996;52:85–87.
218. Lehn J-M. Perspectives in supramolecular chemistry—from molecular recognition towards molecular information processing and self-organization. *Angew Chem Int Ed Engl* 1990;29:1304–1319.
219. Klefenz H. Nanobiotechnology: from molecules to systems. *Eng Life Sci* 2004;4:211–218.
220. Philp D, Stoddart JF. Self-assembly in natural and unnatural systems. *Angew Chem Int Ed Engl* 1996;35:1154–1196.
221. Funeriu DP, Rissanen K, Marie J, Lehn P. Dominant/recessive behavior in the expression of molecular information: self-assembly of inorganic macrocyclic architectures containing coordinatively unsaturated ligands. *Proc Natl Acad Sci USA* 2001;98:10546–10551.
222. Georgakilas V, Pellarini F, Prato M, Guldi DM, Melle-Franco M, Zerbetto F. Supramolecular self-assembled fullerene nanostructures. *Proc Natl Acad Sci USA* 2002;99:5075–5080.
223. Ihara H, Sakurai T, Yamada T, et al. Chirality control of self-assembling organogels from a lipophilic L-glutamide derivative with metal chlorides. *Langmuir* 2002;18:7120–7123.
224. Yao H, Kagoshima Y, Kitamura S, Isohashi T, Ozawa Y, Kimura K. Superstructures of mesoscopic monomolecular sheets of thiacyanine J aggregates in solution. *Langmuir* 2003;19:8882–8887.
225. Derakhshan M, Ansarian H-R, Takafuji M, Sakurai T, Ihara H. The impact of self-assembly in medicine and pharmacology. *Curr Pharm Anal* 2006;2:1–5.
226. Ryu J, Park CB. High-temperature self-assembly of peptides into vertically well-aligned nanowires by aniline vapor. *Adv Mater* 2008;20:3754–3758.
227. Klug A. From macromolecules to biological assemblies (nobel lecture). *Angew Chem Int Ed* 1983;22:565–582.
228. MacKinnon R. Potassium channels and the atomic basis of selective ion conduction (nobel lecture). *Angew Chem Int Ed* 2004;43:4265–4277.
229. Agre P. Aquaporin water channels (nobel lecture). *Angew Chem Int Ed* 2004;43:4278–4290.
230. Wallace BA. Structure of gramicidin A. *Biophys J* 1986;49:295–306.
231. Gouaux E. α-Hemolysin from *Staphylococcus aureus*: an archetype of β-barrel, channel-forming toxins. *J Struct Biol* 1998;121:110–122.
232. Ishii D, Kinbara K, Ishida Y, et al. Chaperonin-mediated stabilization and ATP-triggered release of semiconductor nanoparticles. *Nature* 2003;423:628–632.

233. Bayley H, Cremer PS. Stochastic sensors inspired by biology. *Nature* 2001;413:226–230.
234. Percec V, Dulcey AE, Balagurusamy VSK, et al. Self-assembly of amphiphilic dendritic dipeptides into helical pores. *Nature* 2004;430:764–768.
235. Percec V, Dulcey AE, Peterca M, et al. The internal structure of helical pores self-assembled from dendritic dipeptides is stereochemically programmed and allosterically regulated. *Angew Chem Int Ed* 2005;44:6516–6521.
236. Percec V, Dulcey AE, Peterca M, et al. Principles of self-assembly of helical pores from dendritic dipeptides. *Proc Natl Acad Sci USA* 2006;103:2518–2523.
237. Percec V, Dulcey AE, Peterca M, Ilies M, Sienkowska MJ, Heiney PA. Programming the internal structure and stability of helical pores self-assembled from dendritic dipeptides via the protective groups of the peptide. *J Am Chem Soc* 2005;127: 17902–17909.
238. Van Herwaarden AH. Nano-calorimetry. In Goodwin A, Marsh KN, Wakeham WA (eds): *Measurement of the Thermodynamic Properties of Single Phase*, *VI*. The Netherlands, Elsevier, 2003; 368–385.
239. Wang L, Lin Q. A MEMS nanocalorimeter for biomolecular characterization. *1st IEEE-NEMS*, Art Num 4134968, 2006; 349–352.
240. Zhang YY, Tadigadapa S. Calorimetric biosensors with integrated microfluidic channels. *Biosens Bioelectron* 2004;19:1733–1743.
241. Wang L, Wang B, Lin Q. Demonstration of MEMS-based differential scanning calorimetry for determining thermodynamic properties of biomolecules. *Sensor Actuat B-Chem* 2008; 134:953–958.
242. Garden JL, Chateau E, Chaussy J. Highly sensitive AC nanocalorimeter for microliter-scale liquids or biological samples. *Appl Phys Lett* 2004;84:3597–3599.
243. Danley RL. *Infrared Heated Differential Scanning Calorimeter*, US Patent 2008 304 542 (A1), 1995.
244. Danley RL. *Infrared Heated Differential Thermal Analyzer*, European Patent 0 660 110 (A1), 1995.
245. Gaisford S, Aubuchan SR, Caullfield PA. Use of IR-heated DSC to detect transitions in amorphous lactose. In: Dalby RN, Byron PR, Peart J, Summan JD, Farr SJ, and Young PM (eds): *Respiratory Drug Delivery*, (1), Virginia Common Wealth University, 2008;837–840.
246. Gaisford S, Buanz ABM, Jethwa N. Characterization of paracetamol form III with rapid-heating DSC. *J Pharm Biomed Anal* 2010; 53:366–370.
247. Gill PS, Sauerbrunn SR, Reading M. Modulated differential scanning calorimetry. *J Therm Anal* 1993;40:931–939.
248. Reading M, Elliott D, Hill VL. A new approach to the calorimetric investigation of physical and chemical transitions. *J Therm Anal* 1993;40:949–955.
249. Reading M, Luget A, Wilson R. Modulated differential scanning calorimetry. *Thermochim Acta* 1994;238:295–307.
250. Reading M. *Method and Apparatus for Gas Flow Modulated Differential Scanning Calorimetry*, US Patent 005 624 187 A, 1997.
251. Lacey AA, Nikolopoulos C, Reading M. A mathematical model for modulated differential scanning calorimetry. *J Therm Anal* 1997;50:279–333.
252. Reading M, Hahn BK. *Method and Apparatus for Modulated Differential Analysis*, US Patent 522 477 5, 1993.
253. Reading M. *Method and Apparatus for Spatially Resolved Modulated Differential Analysis*, US Patent 5 248 199, 1993.
254. Marcus SM, Reading M. *Method and Apparatus for Thermal Conductivity Measurements*, US Patent 5 335 993, 1994.
255. Reading M, Hahn BK. *Method and Apparatus for Modulated Differential Analysis*, US Patent 5 346 306, 1994.
256. Reading M. *Method and Apparatus for AC Differential Thermal Analysis*, US Patent 5 439 291, 1995.
257. TN44 information. TA Instruments, New Castle, DE, USA, http://www.tainst.com.
258. McCluskey PJ, Vlassak JJ. Combinatorial study of nanoscale Ti-Ni-Zr by parallel nano-differential scanning calorimetry. *Symposium A: Combinatorial Methods for High-Throughput Materials Science*, 1024E. Materials Research Society, Warrendale, PA, USA, 2006, A8.4, http://www.mrs.org/s_mrs/doc.asp?CID=11140&DID=201670.
259. McCluskey PJ, Vlassak JJ. Parallel nano-differential scanning calorimetry: a new device for combinatorial analysis of complex nano-scale material systems. *Mater Res Soc Sym Proc* 2006;924: 133–138.
260. Pressure Perturbation Calorimetry (PPC) Accessory. *DSC Application Note*, MicroCal, GE Healthcare, Piscataway, NJ, USA, http://www.microcal.com/products/software-accessories/pressure-perturbation-calorimetry.asp.
261. Chalikian TV, Breslauer KE. On volume changes accompanying conformational transitions of biopolymers. *Biopolymers* 1996;39:619–626.
262. Palma R, Curmi PMG. Computational studies on mutant protein stability: the correlation between surface thermal expansion and protein stability. *Protein Sci* 1999;8:913–920.
263. Mitra L, Smolin N, Ravindra R, Royer C, Winter R. Pressure perturbation calorimetric studies of the solvation properties and the thermal unfolding of proteins in solution—experiments and theoretical interpretation. *Phys Chem* 2006;8:1249–1265.
264. Meersman F, Smeller L, Heremans K. Protein stability and dynamics in the pressure-temperature plane. *Bioch Biophys Acta* 2006;1764:346–354.
265. Dragan AI, Russell DJ, Privalov PL. DNA hydration studied by pressure perturbation scanning microcalorimetry. *Biopolymers* 2008;91:95–101.
266. Chong PL-G, Ravindra R, Khurana M, English V, Winter R. Pressure perturbation and differential scanning calorimetric studies of bipolar tetraether liposomes derived from the thermoacidophilic archaeon sulfolobus acidocaldarius. *Biophys J* 2005;89:1841–1849.
267. Cameron D, Cooper A. Pressure perturbation calorimetry of solvation changes in cyclodextrin complexes. *J Incl Phenom Macrocycl Chem* 2004;44:279–282.
268. Laukkanen A, Valtola L, Winnik FM, Tenhu H. Thermosensitive graft copolymers of an amphiphilic macromonomer and N-vinylcaprolactam: synthesis and solution properties in dilute aqueous solutions below and above the LCST. *Polymer* 2005;46:7055–7065.
269. Bailey NA, Hay JN, Price DM. A study of enthalpic relaxation of poly(ethylene terephthalate) by conventional and modulated temperature DSC. *Thermochim Acta* 2001;367–368:425–431.
270. Vanden Poel G, Mathot VBF. High performance differential scanning calorimetry (HPer DSC): a powerful analytical tool for the study of the metastability of polymers. *Thermochim Acta* 2007;461:107–121.
271. Mathot VBF, Scherrenberg RL, Pijpers TFJ. Metastability and order in linear, branched and copolymerized polyethylenes. *Polymer* 1998;39:4541–4559.
272. Gabbott P, Clarke P, Mann T, Royall P, Shergill S. A high-sensitivity, high-speed DSC technique: measurement of amorphous lactose. *Am Lab* 2003;35:17–22.
273. Pijpers TFJ, Mathot VBF, Goderis B, Scherrenberg RL, van der Vegte EW. High-speed calorimetry for the study of the kinetics of (de)vitrification, crystallization, and melting of macromolecules. *Macromolecules* 2002;35:3601–3613.
274. Mathot VBF, Vanden Poel G, Pijpers TFJ. Improving and speeding up the characterization of substances, materials, and products: benefits and potentials of high-speed DSC. *Am Lab* 2006;38:21–25.

275. Mathot VBF, Goderis B, Reynaers H. Metastability in polymer systems studied under extreme conditions: high pressure, scan-iso T-t ramps and high scanning rates. *Fibres Text East Eur* 2003;11:20–27.
276. Luruli N, Pijpers T, Brüll R, Grumel V, Pasch H, Mathot V. Fractionation of ethylene/1-pentene copolymers using a combination of SEC-FTIR and SEC-HPer DSC. *J Polym Sci B: Polym Phys* 2007;45:2956–2965.
277. Pijpers MFJ, Mathot VBF. Optimization of instrument response and resolution of standard- and high-speed power compensation DSC. *J Therm Anal Calorim* 2008;93:319–327.
278. Vanden Poel G, Mathot VBF. High-speed/high performance differential scanning calorimetry (HPer DSC): temperature calibration in the heating and cooling mode and minimization of thermal lag. *Thermochim Acta* 2006;446:41–54.
279. Mathot VBF. New routes for thermal analysis and calorimetry as applied to polymeric systems. *J Therm Anal Calorim* 2001;64:15–35.
280. Saunders M, Podluii K, Shergill S, Buckton G, Royall P. The potential of high speed DSC (Hyper-DSC) for the detection and quantification of small amounts of amorphous content in predominantly crystalline samples. *Int J Pharm* 2004;274:35–40.
281. Werner E. All systems go: three authors present very different views of the developing field of systems biology. *Nature* 2007;446:493–494.
282. Gill P, Ghaemi A. Nucleic acid isothermal amplification technologies—a review. *Nucleosides Nucleotides Nucleic Acids* 2008;27:224–243.
283. Maghami P, Ranjbar B, Hosseinkhani S, Ghasemi A, Moradi A, Gill P. Relationship between stability and bioluminescence color of firefly luciferase. *Photochem Photobiol Sci* 2010;9:376–383.
284. Makarov AA. Heat denaturation of pepsinogen in a water-ethanol mixture. *FEBS Lett* 1995;357:58–61.
285. Privalov G, Kavina V, Freire E, Privalov PL. Precise scanning calorimeter for studying thermal properties of biological macromolecules in dilute solution. *Anal Biochem* 1995;232:79–85.